DOI: 10.1002/ejoc.200600103

Systematic Studies on Photoluminescence of Oligo(arylene-ethynylene)s: Tunability of Excited States and Derivatization as Luminescent Labeling Probes for Proteins

Yong-Gang Zhi,[a] Siu-Wai Lai,*[a] Queenie K.-W. Chan,[a] Yuen-Chi Law,[a] Glenna S.-M. Tong,[a] and Chi-Ming Che*[a]

Keywords: Oligo(phenylene-ethynylene) / π-Conjugation / Fluorescence / Solvatochromism / Protein-labeling

Functionalized oligo(phenylene-ethynylene)s (OPEs) with different conjugation lengths, *p*-X($C_6H_4C{\equiv}C)_nSiMe_3$ (n = 1–4; X = NH_2, NMe_2, H) were synthesized by Sonogashira coupling of (phenylene-ethynylene)s and 1-iodo-4-(trimethylsilylethynyl)benzene, followed by desilylation of the *p*-substituted (trimethylsilylethynyl)benzenes with potassium hydroxide. The photoluminescent properties for the OPE series with different chain lengths and their solvatochromic responses were examined. The absorption maxima were red-shifted with increasing numbers of –($C_6H_4C{\equiv}C$)– units (n), and a linear plot of the absorption energy maxima vs. 1/n was obtained for each series. The emission spectra in dichloromethane showed a broad and structureless band, the energies of which (in wavenumbers) also fit linearly with 1/n. Both the absorption and emission wavelength maxima of the NH_2- and NMe_2-substituted OPEs exhibited significant solvent dependence, whereas the parent OPEs (X = H) showed only minor shifts of the λ_{max} values in different solvents. Substituent effects upon the photoluminescent characteristics of the OPEs and the tunability of the excited states were examined with the *p*-X($C_6H_4C{\equiv}C)_nSiMe_3$ (n = 2, 3; X = NH_2, NMe_2, H, SMe, OMe, OH, and F) series. The H- and F-substituted counterparts exhibited high-energy vibronically structured emissions attributed to the $^3(\pi\pi^*)$ excited states of the (arylene-ethynylene) backbone. For compounds bearing NH_2 and NMe_2 groups, a broad red-shifted emission with a remarkable Stokes shift from the respective absorption maximum was observed, which can be assigned to an $n \rightarrow \pi^*$ transition. The $n \rightarrow \pi^*$ assignment was supported by MO calculations on the model compounds *p*-X($C_6H_4C{\equiv}C)_2SiH_3$ (X = NH_2, H). Functionalization of the oligo(arylene-ethynylene)s with the *N*-hydroxysuccinimidyl (NHS) moiety enabled covalent attachment of the fluorophore to HSA protein molecules. A series of fluorescent labels, namely *p*-X($C_6H_4C{\equiv}C)_n$-C_6H_4NHS, (n = 1, X = NH_2, NMe_2, SMe, OMe, OH, F; n = 2, X = NH_2, NMe_2) and *p*-$Me_2NC_6H_4C{\equiv}C(C_4H_2S)$-$C{\equiv}CC_6H_4NHS$ were synthesized, and their conjugates with HSA (human serum albumin) were characterized by MALDI-TOF mass spectrometry, UV/Vis absorption spectroscopy, and gel electrophoresis.

Introduction

Oligo(phenylene-ethynylene)s (OPEs) with extended conjugated aromatic systems have shown applications in molecular electronics[1] and nonlinear optics[2] because of their intriguing optical and electronic properties. General synthetic procedures of OPEs involve Pd/Cu-catalyzed coupling and desilylation reactions, which enable high degrees of modification in conjugation length,[1f,1g] terminal substituents,[3] and sensory pendants.[4] Recent photophysical investigations of OPEs have revealed intriguing luminescent properties and high quantum yields,[5–7] and accordingly, OPE materials have been employed in organic electroluminescent light-emitting devices,[8] liquid-crystal displays,[9] and chemosensors[10] for electron-poor aromatics,[11] fluoride ions,[12] biological targets,[13] and metal cations.[14]

The photophysical characteristics of OPEs can be significantly perturbed by different end-capping substituents and the extent of conjugation, and the latter enables electronic communication across a linear OPE chain over a long distance.[15,16] Herein is described the synthesis and photophysical properties of conjugated OPE materials with progressively increasing chain length and different terminal groups. The correlation between photoluminescent characteristics and conjugation length is presented, and through studying the electronic excited states of the conjugated oligomers, the effect of remote terminal electron-donating substituents upon the nature of the excited state is elucidated. Through derivatization of the oligo(arylene-ethynylene)s with the lysine-reactive *N*-hydroxysuccinimidyl (NHS)

[a] Department of Chemistry, HKU-CAS Joint Laboratory on New Materials and Open Laboratory of Chemical Biology of the Institute of Molecular Technology for Drug Discovery and Synthesis, The University of Hong Kong,
Pokfulam Road, Hong Kong SAR, China
Fax: +852-2857-1586
E-mail: cmche@hku.hk
swlai@hku.hk

Supporting information for this article is available on the WWW under http://www.eurjoc.org or from the author.

moiety, we have been able to covalently attach the non-toxic OPEs as strongly fluorescent labels to the HSA (human serum albumin) biomolecules used in this work.

Results and Discussion

Synthesis and Characterization

Figure 1 depicts the oligo(arylene-trimethylsilylethynylene)s containing $-(C_6H_4C{\equiv}C)_n-$ chains (n = 1–4) with the terminal *para* substituents NH_2 (**1a**–**4a**) and NMe_2 (**1b**–**4b**). For comparison, the unsubstituted parent derivatives (**1h**–**4h**) have also been prepared. Scheme 1 outlines the synthetic routes for **1a**–**4a** and **1b**–**4b**, which involve Sonogashira[17] coupling of (arylene-ethynylene)s with 1-iodo-4-(trimethylsilylethynyl)benzene in the presence of CuI and $Pd(PPh_3)_2Cl_2$ as catalysts and $NHEt_2$ as base, followed by the desilylation of the *p*-substituted (trimethylsilylethynyl)-benzenes with potassium hydroxide. These procedures have been adopted for the preparation of OPEs and their oligomers.[1b,1e,18–23]

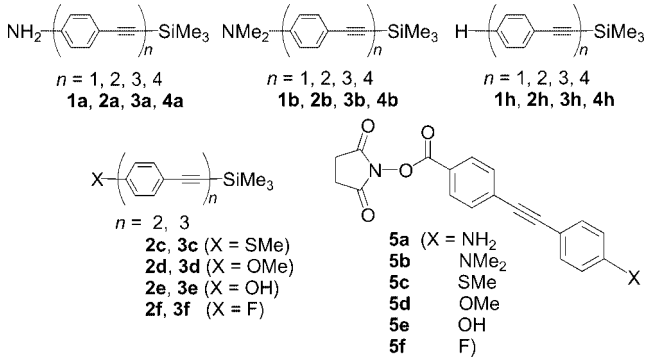

Figure 1. Structures of oligo(arylene-trimethylsilylethynylene)s and NHS-capped diphenylacetylenes.

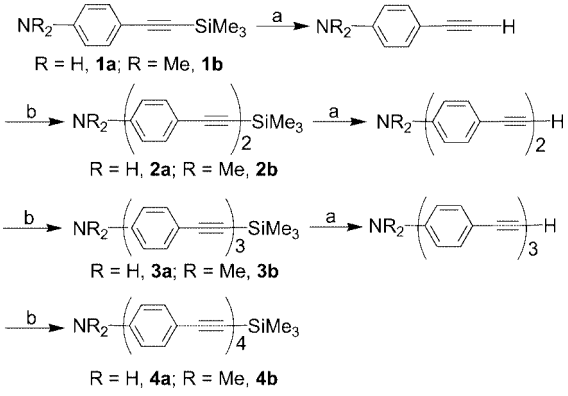

Scheme 1. Synthesis of **1a**–**4a** and **1b**–**4b**: a) 1.1 equiv. of KOH in MeOH/THF, 25 °C, 4 h; b) $Pd(PPh_3)_2Cl_2$ (2 mol-%), CuI (1 mol-%), 1-iodo-4-(trimethylsilylethynyl)benzene (0.91 equiv.), and $NHEt_2$ in THF, 25 °C, 24 h.

Substituent effects were also investigated by preparing two series of compounds p-$X(C_6H_4C{\equiv}C)_nSiMe_3$ [n = 2, 3; X = NH_2 (**2a**, **3a**), NMe_2 (**2b**, **3b**), H (**2h**, **3h**), SMe (**2c**, **3c**), OMe (**2d**, **3d**), OH (**2e**, **3e**), F (**2f**, **3f**)]. *N*-Hydroxysuccinimidyl (NHS) ester derivatives of diphenylacetylenes, **5a**–**5f**, were synthesized by reaction of succinimidyl 4-iodobenzoate with p-$X(C_6H_4C{\equiv}C)H$ (X = NH_2, NMe_2, SMe, OMe, OH, F) (Scheme 2). Similarly, p-$X(C_6H_4C{\equiv}C)_2C_6H_4NHS$ (X = NH_2, NMe_2), and p-$Me_2NC_6H_4C{\equiv}C(C_4H_2S)$-$C{\equiv}CC_6H_4NHS$ were obtained using p-$X(C_6H_4C{\equiv}C)_2H$ and p-$Me_2NC_6H_4C{\equiv}C(C_4H_2S)C{\equiv}CH$, respectively. The NHS moiety is capable of reacting with lysine and α-amino groups of proteins, such as HSA in this work, which has resulted in the covalent attachment of fluorescent oligo-(arylene-ethynylene)s to biomolecules.

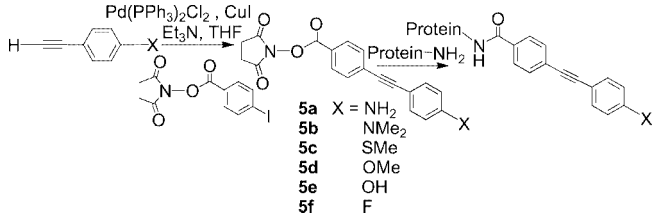

Scheme 2. Synthesis of NHS-capped diphenylacetylenes bearing different *para* substituents, **5a**–**5f**, and coordinative attachment of fluorophores to protein molecules.

Compounds **3a**, **4a**, **2b**–**4b**, **2c**–**2f**, **3c**–**3f**, and **5a**–**5f** were prepared by high-yielding reactions, and have been characterized by ^1H and ^{13}C NMR and high-resolution electron ionization (EI) mass spectrometry. All compounds are stable in the solid state and in solution. For p-$X(C_6H_4C{\equiv}C)_nSiMe_3$ (X = NH_2, **1a**–**4a**; X = NMe_2, **1b**–**4b**), the first three compounds (n = 1–3) of each series exhibit good solubility in common solvents. However, the p-$X(C_6H_4C{\equiv}C)_4SiMe_3$ compounds are barely soluble in dichloromethane, chloroform, DMF and DMSO, and only sparingly soluble in *n*-hexane, methanol, and acetonitrile. Similarly, for $H(C_6H_4C{\equiv}C)_nSiMe_3$ (**1h**–**4h**), compounds **1h** and **2h** are soluble in most solvents, whereas **4h** is only soluble in toluene and dichloromethane.

Phase Transition, Thermo- and Photostability

Samples for differential scanning calorimetric (DSC) studies and thermogravimetric analysis (TGA) were dried under vacuum for 24 h. The DSC thermograms of **2a**, **3a** and **1b**–**3b** are shown in Figures S1 and S2 of the Supporting Information. For **2a**, an endothermic maximum at 153 °C was observed, but upon increasing the chain length for **3a**, a higher transition temperature of 234 °C (with decreased magnitude of the melting peak) was observed. Similar results were found for **1b**–**3b**, with the peak temperature progressively increasing from 96 (**1b**) to 132 (**2b**) and 216 °C (**3b**). The values of the enthalpy of transition (ΔH) for **1b** and **2b** are 19.4 and 18.0 kJ/mol, respectively, whereas that of **3b** is increased to 36.8 kJ/mol. The TGA thermograms

of **3a**, **4a**, and **2b**–**4b** (Figures S3 and S4) reveal that they are stable up to 245, 273, 241, 299, and 295 °C, respectively. The photostability of **5b** in acetonitrile was examined: no detectable changes in absorption and emission spectra in acetonitrile solution were observed under ambient light and air for a week. However, irradiation with a high-power, broad-band mercury arc lamp (500 W) for 2.5 h under air resulted in blue-shifted absorption maxima, from 277 and 378 nm to 271 and 351 nm, accompanied by a gradual decrease in absorbance, by 28 and 42%, respectively.

Absorption and Emission Spectroscopy

The UV/Vis absorption and emission data of **1a**–**4a**, **1b**–**4b**, **1h**–**4h**, **2c**–**2f**, **3c**–**3f**, **5a**–**5f** and *p*-$Me_2NC_6H_4C{\equiv}C(C_4H_2S)C{\equiv}CC_6H_4NHS$ in various solvents are listed in Table 1 (details in the Supporting Information). Our intention is to examine the effect of (A) chain length, (B) solvent polarity, and (C) *para* substituent upon the electronic excited states of (arylene-ethynylene)s.

(A) Effect of Increasing Chain Length

Figure 2 shows the absorption spectra of **1a**–**4a** in dichloromethane at 298 K. Upon lengthening of the conjugation of *p*-$H_2N(C_6H_4C{\equiv}C)_nSiMe_3$ (**1a**–**4a**) chain (from n = 1 to 4), the π-π* absorption band[24] of **1a** at λ_{max} = 278 nm (ε = 2.81×10^4 $dm^3\,mol^{-1}\,cm^{-1}$) in CH_2Cl_2 shows a bathochromic shift with progressively increased ε value to λ_{max} = 331, 345, and 356 nm [ε = (3.62, 5.88, and 8.89)$\times10^4$ $dm^3\,mol^{-1}\,cm^{-1}$] for **2a**–**4a**, respectively. The red-shifted absorption maximum for increasing n is consistent with greater π-conjugation upon lengthening of the arylene-ethynylene chain.[25] Interestingly, a plot of the absorption maximum (in wavenumber) vs. 1/n affords a linear fit (inset of Figure 2), and as $n\rightarrow\infty$, the absorption maximum approaches the limiting value of 25330 cm^{-1} (λ_{max} = 395 nm). The molar extinction coefficients (ε) of the lowest-energy transition of **1a**–**4a** also increase from n = 1 to 4. In the absorption spectrum of **2a** in dichloromethane, additional well-resolved vibronic absorption bands at λ_{max} = 276 and 288 nm are observed besides the major peak maximum at 331 nm. These high-energy absorption bands become broad and less resolved as the conjugation length increases, as in the cases of **3a** and **4a**.

Excitation of **1a**–**4a** at 280–360 nm in dichloromethane at 298 K produces a blue-green or green emission (Table 1). Upon increasing of the chain length, the emission λ_{max} red-shifts from 342 nm for **1a**, to 415 nm for **2a**, 457 nm for **3a**, and 471 nm for **4a** (Figure 3). This is reminiscent of the bathochromic shift in the corresponding absorption spectra (Figure 2). A plot of the emission maximum (in wavenumber) vs. 1/n shows a linear fit (inset of Figure 3), and the emission maximum apparently reaches a limit of ca. 540 nm as $n\rightarrow\infty$. When monitoring the emission wavelength at 342 nm, the excitation spectrum of **1a** in dichloromethane exhibits an intense band at 278 nm, which matches the ground-state absorption depicted in Figure 2. Likewise, the excitation spectra of **2a**–**4a** are identical to their respective absorption spectra. The emission quantum yield in dichloromethane varies from 0.023 (**1a**) to 0.84 (**3a**).

For the *p*-$Me_2N(C_6H_4C{\equiv}C)_nSiMe_3$ (**1b**–**4b**; n = 1–4) series, the red-shifted π-π* absorption band in CH_2Cl_2 solution appears at λ_{max} = 298, 356, 369, and 370 nm [ε = (3.53, 4.04, 6.16, and 7.88)$\times10^4$ $dm^3\,mol^{-1}\,cm^{-1}$] for **1b**–**4b**, respectively (Figure S5). The ε values at λ_{max} for **1b**–**4b** increase along the series, like for **1a**–**4a**. The absorption spectrum of **2b** in dichloromethane exhibits well-resolved absorption peak maxima at 275–291 nm plus a 356 nm absorption maximum. The absorption spectrum of **4b** in various solvents features one broad band at λ_{max} = 364–371 nm.

Emission data of **1b**–**4b** in various solvents at 298 K are summarized in Table 1. Emission spectra of **2b**–**4b** in hexane exhibit vibronically structured bands with peak maxima at 366–401 nm. The emission spectra of **1b**–**4b** in other solvents are broad and structureless. In CH_2Cl_2, the emission λ_{max} red-shifts from 362, to 440, 488, and 510 nm for **1b**–**4b**, respectively. A plot of the emission energy vs. 1/n is linear (Supporting Information, Figure S6), and the emission approaches the limit of 586 nm as $n\rightarrow\infty$. In CH_2Cl_2, the emission quantum yields show a similar trend to **1a**–**4a**, and differ between 0.025 for **1b** and 0.72 for **3b**, while the lifetime measurement varies from 0.35 (**1b**) to 1.95 ns (**3b**).

For the parent $H(C_6H_4C{\equiv}C)_nSiMe_3$ (**1h**–**4h**; n = 1–4) series, the π-π* absorptions in several solvents show vibronically structured bands (Figure 4), which become less resolved with increasing n. The absorption maxima of **2h** in dichloromethane appear at 303 and 323 nm [ε = (4.69 and 4.48)$\times10^4$ $dm^3\,mol^{-1}\,cm^{-1}$], and are red-shifted from those of **1h** at 248 and 260 nm [ε = (2.82 and 2.50)$\times10^4$ $dm^3\,mol^{-1}\,cm^{-1}$]. The λ_{max} values of **3h** and **4h** are further red-shifted to 332 (ε = 6.95×10^4 $dm^3\,mol^{-1}\,cm^{-1}$) and 345 nm (ε = 9.39×10^4 $dm^3\,mol^{-1}\,cm^{-1}$), respectively. The magnitude of the red shift in λ_{max} for n = 1 to 4, from **1h** to **4h**, is 11340 cm^{-1}, which is larger than the corresponding shift of 7880 and 6530 cm^{-1} from **1a** to **4a** and from **1b** to **4b**, respectively. A plot of the absorption energies for **1h**–**4h** in CH_2Cl_2 vs. 1/n is linear, and gives a limiting energy of 25200 cm^{-1} (397 nm) at $n\rightarrow\infty$ (inset of Figure 4), whereas the ε_{max} values are observed to increase with n (Supporting Information, Figure S7).

The emission spectra of **1h**–**4h** in various solvents are vibronically structured. The emission maximum of **1h** in dichloromethane occurs at the 0–1 transition of 299 nm, whereas those of **2h**–**4h** gradually shift to the 0–0 transition at 328, 364 and 383 nm, respectively. Hence, the relative intensity of the 0–0 transition increases with n, while that of the 0–1 transition decreases. This is indicative of an increase in intrachain coupling interaction(s) with greater conjugation.[26] The 0–0 emission peak (in wavenumbers) of **1h**–**4h** in dichloromethane follows a linear relationship with 1/n (Supporting Information, Figure S8), and the λ_{max} value approaches 416 nm as $n\rightarrow\infty$. The quantum yield of **1h** in dichloromethane is relatively low (0.04) compared to those of **2h**–**4h** (0.55–0.78).

Table 1. Photophysical data for oligo(arylene-ethynylene)s in various solvents at 298 K.

Compound	Medium	λ_{abs}/nm (ε/dm^3 mol^{-1} cm^{-1})[a]	λ_{em}/nm; Φ[a]	$\Delta\nu$ [cm^{-1}][b]
p-$H_2N(C_6H_4C{\equiv}C)SiMe_3$ (**1a**)	*n*-hexane	273 (28000)	332; 0.28	6510
	Et_2O	280 (32720)	344; 0.20	6645
	CH_2Cl_2	278 (28100)	342; 0.023	6732
	CH_3OH	279 (26400)	351; 0.013	7352
	CH_3CN	281 (31600)	346; 0.075	6686
p-$H_2N(C_6H_4C{\equiv}C)_2SiMe_3$ (**2a**)	*n*-hexane	273 (24600), 285 (28300), *322* (47900), 333 (sh, 42500), 343 (41300)	351, *372* (max); 0.54	4174
	$C_6H_5CH_3$	*332* (34800), 349 (sh, 31000)	392; 0.47	4610
	Et_2O	274 (23900), 286 (24400), *337* (35800)	408; 0.28	5164
	CH_2Cl_2	276 (19700), 288 (21900), *331* (36200), 343 (sh, 34800)	415; 0.34; τ[c] = 1.14 ns	6115
	CH_3OH	274 (25100), 286 (26700), *335* (42500)	440; 0.008	7124
	MeCN	275 (21500), 286 (22600), *339* (37400)	469; 0.071	8177
p-$H_2N(C_6H_4C{\equiv}C)_3SiMe_3$ (**3a**)	*n*-hexane	*342* (53300), 366 (sh, 32300)	*377* (max), 397; 0.83	2715
	$C_6H_5CH_3$	347 (57700)	416; 0.88	4780
	Et_2O	351 (58900)	441; 0.81	5814
	CH_2Cl_2	345 (58800)	457; 0.84	7104
	CH_3OH	341 (60600)	514; 0.047	9870
	CH_3CN	348 (54100)	520; 0.14	9505
p-$H_2N(C_6H_4C{\equiv}C)_4SiMe_3$ (**4a**)	$C_6H_5CH_3$	356 (88600)	417; 0.79	4268
	Et_2O	275 (31000), *356* (80910)	462; 0.68	6445
	CH_2Cl_2	275 (27400), *356* (88850)	471; 0.63	6859
p-$Me_2N(C_6H_4C{\equiv}C)SiMe_3$ (**1b**)	*n*-hexane	*289* (35000), 297 (sh, 32600)	346; 0.24	5700
	$C_6H_5CH_3$	*294* (42200), 307 (sh, 34300)	355; 0.14	5845
	Et_2O	*291* (35500), 299 (sh, 33600)	353; 0.16	6036
	CH_2Cl_2	*298* (35300), 305 (sh, 34100)	362; 0.025; τ[d] = 0.35 ns	5933
	CH_3OH	294 (33400)	359; 0.020	6159
	CH_3CN	297 (34400)	364; 0.16	6198
p-$Me_2N(C_6H_4C{\equiv}C)_2SiMe_3$ (**2b**)	*n*-hexane	273 (26400), 278 (27100), 289 (28600), *339* (48300), 361 (45300)	*366* (max), 384; 0.69; τ[c] = 0.88 ns	2176
	$C_6H_5CH_3$	354 (42700)	402; 0.62; τ[c] = 0.94 ns	3373
	Et_2O	273 (30100), 279 (30300), 288 (30000), *349* (48600)	411; 0.60; τ[c] = 1.13 ns	4322
	CH_2Cl_2	275 (25000), 283 (sh, 25500), 291 (26300), 305 (sh, 19600), 327 (30200), *356* (40400)	440; 0.44; τ[c] = 1.88 ns	5363
	CH_3OH	273 (26300), 279 (26400), 288 (26200), *350* (44800)	482; 0.014	7825
	CH_3CN	274 (28600), 281 (28800), 289 (28800), 324 (sh, 29500), *356* (47100)	486; 0.14; τ[c] = 2.21 ns	7514
p-$Me_2N(C_6H_4C{\equiv}C)_3SiMe_3$ (**3b**)	*n*-hexane	259 (15500), 290 (25100), 298 (25900), 312 (sh, 30800), 322 (33100), 341 (sh, 44000), *359* (51200)	*392* (max), 412, 429 (sh); 0.77	2345
	$C_6H_5CH_3$	319 (47200), 326 (47200), 345 (sh, 52000), *368* (65800)	427; 0.84	3755
	Et_2O	259 (20300), 291 (33900), 297 (34900), 317 (41200), 324 (41500), 341 (sh, 50200), *362* (59900)	447; 0.81	5253
	CH_2Cl_2	262 (20400), 293 (sh, 35900), 301 (sh, 38900), 320 (46600), 327 (46300), 344 (sh, 50100), *369* (61600)	488; 0.72; τ[c] = 1.95 ns	6609
	CH_3OH	259 (17600), 290 (sh, 30700), 299 (sh, 32800), 316 (38400), 325 (sh, 37600), 339 (sh, 42700), *361* (53300)	522; 0.084	8544
	CH_3CN	260 (23300), 298 (sh, 42000), 316 (47600), 323 (sh, 46200), 340 (sh, 49600), *368* (66700)	545; 0.11	8825

Table 1. *(Continued)*

Compound	Medium	λ_{abs}/nm (ε/dm^3 mol^{-1} cm^{-1})[a]	λ_{em}/nm; Φ[a]	$\Delta\nu$ [cm^{-1}][b]
p-$Me_2N(C_6H_4C{\equiv}C)_4SiMe_3$ (**4b**)	$C_6H_5CH_3$	323 (sh, 51500), 346 (66100), *371* (73000)	439; 0.75	5311
	Et_2O	342 (sh, 68200), *364* (75900)	468; 0.72	6105
	CH_2Cl_2	347 (sh, 69800), *370* (78800)	510; 0.58; τ[c] = 1.58 ns	7419
p-$MeS(C_6H_4C{\equiv}C)_2SiMe_3$ (**2c**)	CH_2Cl_2	292 (sh, 31700), *324* (55500), 342 (51100)	387; 0.70; τ[d] = 0.82 ns	5024
p-$MeO(C_6H_4C{\equiv}C)_2SiMe_3$ (**2d**)	CH_2Cl_2	*313* (51800), 332 (45100)	371; 0.39; τ[d] = 0.59 ns	4995
p-$HO(C_6H_4C{\equiv}C)_2SiMe_3$ (**2e**)	CH_2Cl_2	292 (sh, 27300), *310* (37500), 329 (32600)	367; 0.38; τ[d] = 0.55 ns	5010
p-$F(C_6H_4C{\equiv}C)_2SiMe_3$ (**2f**)	CH_2Cl_2	261 (sh, 13300), 289 (sh, 35300), *302* (45500), 311 (sh, 37700), 321 (43400), 340 (sh, 3350)	328, *345* (max); 0.38; τ[d] = 0.56 ns	4127
p-$H_2N(C_6H_4C{\equiv}C)C_6H_4$–NHS (**5a**)	CH_2Cl_2	271 (12400), *354* (19400)	495; 0.095	8047
	CH_3CN	269 (19800), *358* (26500)	490; 0.001	7525
	THF	273 (19100), *366* (26800)	500; 0.058	7322
	EA	271 (20300), *359* (29000)	504; 0.034	8014
	DMF/H_2O	260 (14500), *320* (15100)	476; 0.0021	10242
	DMF/PBS	260 (14300), *320* (15400)	475; 0.0017	10197
5a–HSA conjugate	PBS	275, *328*	475; 0.061	9435
p-$Me_2N(C_6H_4C{\equiv}C)C_6H_4$–NHS (**5b**)	DMF/PBS	263 (16200), *343* (17100)	515; 0.0036	9737
5b–HSA conjugate	PBS	278, *345*	480; 0.13	8152
p-$MeS(C_6H_4C{\equiv}C)C_6H_4$–NHS (**5c**)	DMF/PBS	252 (18900), 278 (12800), *311* (21400)	451; 0.041	9981
5c–HSA conjugate	PBS	269 (sh), 286, *322*	419; 0.29	7190
p-$MeO(C_6H_4C{\equiv}C)C_6H_4$–NHS (**5d**)	DMF/PBS	265 (9200), *307* (18900)	418; 0.059	8650
5d–HSA conjugate	PBS	259, 275 (sh), 287 (sh), *308*	409; 0.25	8018
p-$HO(C_6H_4C{\equiv}C)C_6H_4$–NHS (**5e**)	DMF/PBS	280 (10800), *327* (14800)	420; 0.0017	6772
5e–HSA conjugate	PBS	260 (sh), 278, 286 (sh), *308*	409; 0.020	8018
p-$F(C_6H_4C{\equiv}C)C_6H_4$–NHS (**5f**)	DMF/PBS	*309* (18300)	419; 0.11	8496
5f–HSA conjugate	PBS	*293*, 313 (sh)	364; 0.065	6657
p-$Me_2NC_6H_4C{\equiv}C(C_4H_2S)C{\equiv}CC_6H_4$–NHS	DMF/PBS	267 (sh, 14600), 307 (11300), *344* (13400), 383 (10900)	572; 0.001	11587
p-$Me_2NC_6H_4C{\equiv}C(C_4H_2S)C{\equiv}CC_6H_4$–NHS–HSA conjugate	PBS	271, *362*	511; 0.10	8055

[a] Numbers in *italic* indicate the most intense bands. [b] $\Delta\nu$ is the difference between the absorption and emission maximum in wavenumber. [c] The lifetime measurement was performed using a 373 nm laser source. [d] The lifetime measurement was performed using a 295 nm laser source.

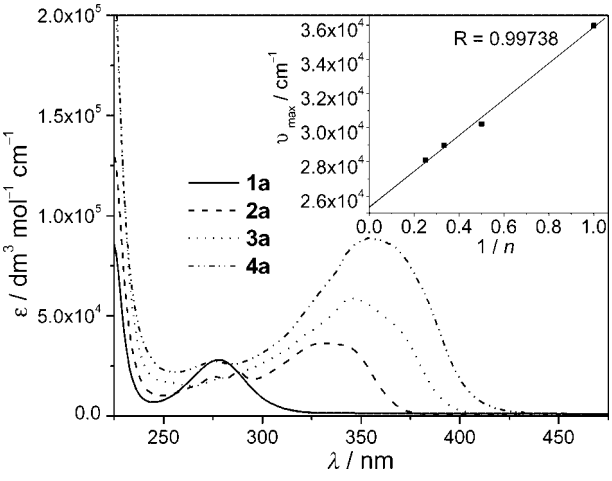

Figure 2. UV/Vis absorption spectra of **1a**–**4a** in dichloromethane at 298 K. Inset: plot of $\tilde{\nu}_{max}$ [cm^{-1}] vs. 1/*n*.

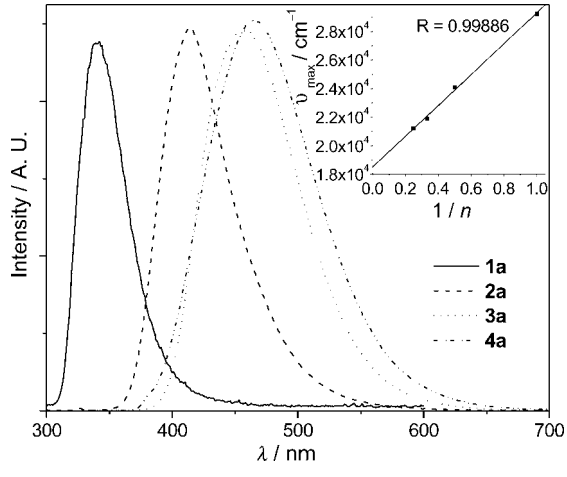

Figure 3. Emission spectra of **1a**–**4a** in dichloromethane at 298 K (concentration = 2×10^{-5} mol dm^{-3}, λ_{ex} = 280–360 nm). Inset: plot of $\tilde{\nu}_{max}$ [cm^{-1}] vs. 1/*n*.

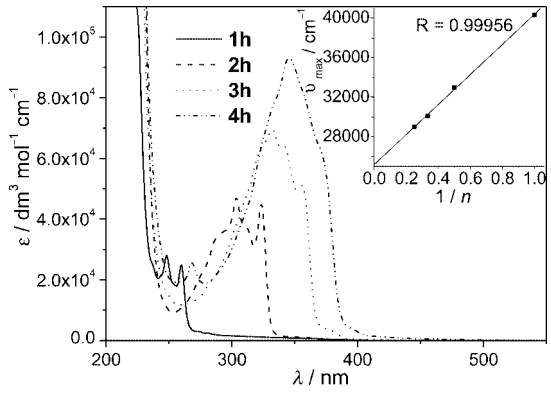

Figure 4. UV/Vis absorption spectra of **1h**–**4h** in dichloromethane at 298 K. Inset: plot of absorption maximum in $\tilde{\nu}_{max}$ [cm^{-1}] vs. $1/n$ for $H(C_6H_4C{\equiv}C)_nSiMe_3$ (**1h**–**4h**).

(B) Effect of Solvent Polarity

The absorption spectra of **1a**–**4a** are moderately sensitive to solvent polarity. For example, the absorption band of **1a** at 273 nm in hexane red-shifts to 281 nm in acetonitrile, whereas that of **3a** shows a solvatochromic shift from 342 nm in hexane to 351 nm in diethyl ether. *p*-$H_2N(C_6H_4C{\equiv}C)_2SiMe_3$ (**2a**) exhibits the largest solvatochromic effect; the π-π* absorption maximum (λ_{max}) shifts from 322 nm ($\varepsilon = 4.79\times10^4$ $dm^3\,mol^{-1}\,cm^{-1}$) in hexane to 339 nm ($\varepsilon = 3.74\times10^4$ $dm^3\,mol^{-1}\,cm^{-1}$) in acetonitrile. The low solubility of **4a** limits the solvents that can be employed for solvatochromic studies; this compound is only sparingly soluble in toluene, diethyl ether and dichloromethane.

The emission spectra of **2a**–**4a** in hexane show vibronically structured bands. For **3a**, the peak maxima appear at 377 and 397 nm, with vibrational progression of ca. 1340 cm^{-1}, which corresponds to a combination of phenyl ring deformation and symmetric phenyl ring and C≡C stretches.[23] Likewise, *p*-$H_2N(C_6H_4C{\equiv}C)_4SiMe_3$ (**4a**) in hexane shows vibronically structured bands with peak maxima at 388 and 404 nm, with vibrational progression of ca. 1020 cm^{-1}. Like **1h**–**4h**, the relative intensity of the 0–0 transition increases with n, while that of the 0–1 transition decreases. Red-shifted emission maxima from 372 for **2a** to 377 and 388 nm for **3a** and **4a**, respectively, have been observed in hexane. In other solvents, the emission of **1a**–**4a** is usually broad and structureless. In acetonitrile, **3a** shows a broad emission with λ_{max} = 520 nm, which is red-shifted by 7290 cm^{-1} from its 377 nm emission in hexane, affording the greatest solvatochromic shift. The quantum yields of **3a** in hexane, toluene, diethyl ether and dichloromethane are comparable (0.81–0.88), whereas those in methanol (0.047) and acetonitrile (0.14) are substantially lower.

Effect of solvent upon the emission of **2a** (concentration: 2×10^{-5} $mol\,dm^{-3}$) has been examined in detail (Table 1). Both the emission maximum (λ_{max}) and quantum yield (Φ) are sensitive to solvent polarity; λ_{max} varies from 372 nm in hexane to 469 nm in acetonitrile, while Φ decreases from 0.54 in hexane to 0.008 in methanol. We have observed a linear correlation between the solvent polarity, defined by the E_T value (classified with respect to the longest-wavelength solvatochromic absorption band of the pyridinium *N*-phenolate betaine dye), and the emission quantum yield of **2b**, as depicted in Figure 5. Plots of emission maximum (in wavenumber) and lifetime for **2b** against E_T also show reasonably linear relationships (Figures S9 and S10, respectively).

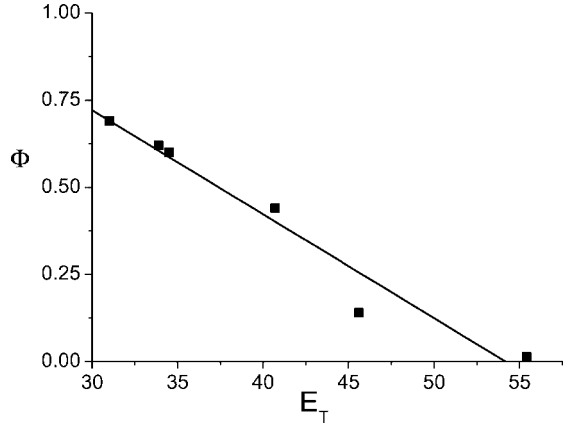

Figure 5. Plot of emission quantum yield for **2b** in various solvents against the E_T value.

The π → π* transitions in the absorption spectra of **1b**–**4b** show moderate sensitivity toward solvent polarity; *p*-$Me_2N(C_6H_4C{\equiv}C)_2SiMe_3$ (**2b**) exhibits the largest solvatochromic shift and its peak maximum at 339 nm in hexane red-shifts to 356 nm in dichloromethane. The highest energy absorption maximum of **1b** (289 nm) and **3b** (359 nm) in hexane are red-shifted only slightly to 298 and 369 nm, respectively, in dichloromethane. In contrast, the emission spectra of **2b**–**4b** show more significant solvatochromic shifts. The emission spectra of **2b**–**4b** in hexane show vibronic bands with peaks at 366 and 384 nm for **2b**, 392 and 412 nm for **3b**, and 404 and 426 nm for **4b**. The vibrational spacings of 1240–1280 cm^{-1} can be attributed to a combination of phenyl ring deformation and symmetric phenyl ring and C≡C stretches.[23] However, the emissions become broad and structureless in toluene and acetonitrile. The 439 nm emission for **4b** in toluene shows a bathochromic shift to 510 nm in dichloromethane. The largest red-shift of the emission maximum was observed for **3b**, changing from λ_{max} = 392 nm in hexane to 545 nm in acetonitrile ($\Delta\nu$ = 7160 cm^{-1}); the emission of **2b** also changes significantly from 366 nm in hexane to 486 nm in acetonitrile ($\Delta\nu$ = 6750 cm^{-1}). The quantum yields of **2b** and **3b** in hexane, toluene, diethyl ether and dichloromethane lie in the range of 0.44–0.69 and 0.72–0.84, respectively, but in methanol and acetonitrile, the quantum yields decreased to 0.014–0.14. This highlights the remarkable effects of solvent polarity upon the spectroscopic properties of these compounds. Self-quenching experiments on the emission of **2b** were performed in the concentration range of 4.1×10^{-7}–3.2×10^{-4} $mol\,dm^{-3}$ in CH_2Cl_2 at 298 K, but no detectable quenching effect was found.

The absorption maxima of **1h**–**4h** show relatively small bathochromic shifts with solvent polarity (Supporting Information) compared to **1a**–**4a** and **1b**–**4b**. The maximum

solvatochromic shift is only 4 nm for **3h** (λ_{max} = 328 nm in diethyl ether to 332 nm in dichloromethane). The emission spectra of **1h**–**4h** also show little variation in peak maximum and quantum yield with solvent; **3h** shows emission spectra with λ_{max} = 358–364 nm and a quantum yield of 0.69–0.86 despite the solvent changing from hexane to dichloromethane and toluene.

(C) Effect of the para Substituent in the Oligo(arylene-ethynylene)s

We have examined the effect of different *para* substituents upon the photoluminescent properties of *p*-$X(C_6H_4C{\equiv}C)_nSiMe_3$ [*n* = 2, 3; X = NH_2 (**2a**, **3a**), NMe_2 (**2b**, **3b**), H (**2h**, **3h**), SMe (**2c**, **3c**), OMe (**2d**, **3d**), OH (**2e**, **3e**), F (**2f**, **3f**)]. Figure 6 depicts the absorption spectra of **2a**–**2f** and **2h** in dichloromethane at 298 K. Compounds **2h** and **2c**–**2f** exhibit vibronically structured π-π* absorption bands with λ_{max} = 302–324 nm [ε = (3.8–5.6) × 10^4 $dm^3\,mol^{-1}\,cm^{-1}$]. For compounds bearing NH_2 (**2a**) and NMe_2 (**2b**) substituents, there is a broad low-energy π-π* absorption band with λ_{max} = 331 and 356 nm [ε = (3.62 and 4.04) × 10^4 $dm^3\,mol^{-1}\,cm^{-1}$], respectively, in addition to the vibronically structured bands at λ_{max} = 275–291 nm [ε = (1.97–2.63) × 10^4 $dm^3\,mol^{-1}\,cm^{-1}$]. Among the *p*-substituted derivatives, the SMe congener (**2c**) has the highest molar extinction coefficients.

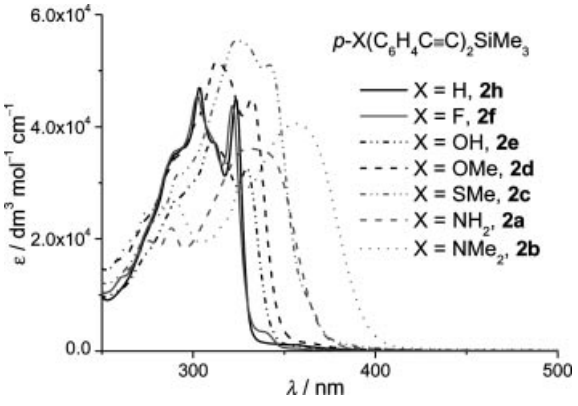

Figure 6. UV/Vis absorption spectra of **2a**–**2f** and **2h** in dichloromethane at 298 K.

The emissions of **2a**–**2f** and **2h** in dichloromethane at 298 K have also been examined (Figure 7). The emission spectrum of $H(C_6H_4C{\equiv}C)_2SiMe_3$ (**2h**) exhibits vibronically structured bands, which are attributed to the $^3(\pi\text{-}\pi^*)$ excited states of the diphenylacetylene. The Stokes shift between the emission maximum of **2h** at 328 nm from its absorption maximum at 303 nm in dichloromethane is 2520 cm^{-1}, which matches those for typical $^1(\pi\text{-}\pi^*)$ excited states.[24] Similar spectral features have also been found for **2f** with the Stokes shift being 4130 cm^{-1}. The emissions of **2a**–**2e** in dichloromethane are broad, with λ_{max} ranging from 367 (**2e**) to 440 nm (**2b**) (Table 1). The Stokes shifts between the π-π* absorption and emission energies for **2a**–**2e** are larger than those for **2f** and **2h**. We tentatively assign the emission of **2a**–**2e** to originate from n → π* transitions. The emission maxima (λ_{max}) for **2a**–**2f** and **2h** follow a similar trend to their absorption energies; NH_2- (**2a**) and NMe_2-substituted (**2b**) compounds emit at λ_{max} = 415 and 440 nm, respectively, which are red-shifted from those observed for **2c**–**2f** and **2h**. The quantum yields of **2a**–**2f** and **2h** lie in the range of 0.34–0.70, with the highest value found for the SMe counterpart (**2c**), while their fluorescent lifetimes measured in CH_2Cl_2 range from 0.55 to 1.88 ns.

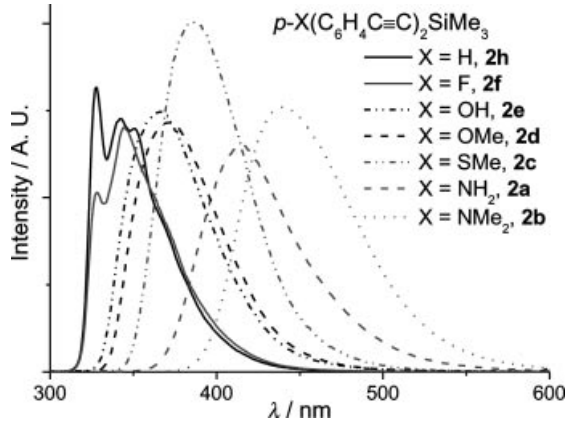

Figure 7. Emission spectra of **2a**–**2f** and **2h** in dichloromethane at 298 K (concentration = 2×10^{-5} mol dm^{-3}, λ_{ex} = 280–360 nm).

The absorption spectra of *p*-$X(C_6H_4C{\equiv}C)_3SiMe_3$ [X = NH_2 (**3a**), NMe_2 (**3b**), H (**3h**), SMe (**3c**), OMe (**3d**), OH (**3e**), F (**3f**)] in dichloromethane are shown in the Supporting Information (Figure S11). Compounds **3h** and **3f** exhibit a vibronically structured π-π* absorption band at λ_{max} ≈ 332 nm [ε = (6.95 and 6.02) × 10^4 $dm^3\,mol^{-1}\,cm^{-1}$, respectively], while **3a**–**3e** show a broad π-π* absorption band at 336–369 nm [ε = (5.88–8.08) × 10^4 $dm^3\,mol^{-1}\,cm^{-1}$] in dichloromethane. The emission spectra of **3a**–**3f** and **3h** in dichloromethane are shown in Figure S12. Upon excitation at 330 nm, the emission of **3h** and **3f** are vibronically structured with peak maxima at ca. 362 nm and quantum yields of 0.78–0.80. The Stokes shifts (around 2600 cm^{-1}) for **3h** and **3f** are consistent with the $^3(\pi\text{-}\pi^*)$ excited states of arylene-ethynylenes. For other *para*-substituted congeners (**3c**–**3e**), single emission bands were observed at λ_{max} = 394–410 nm with quantum yields of 0.83–0.85. The intensely emissive SMe-substituted **3c** displays the highest Φ value of 0.85. For amino- and dimethylamino-substituted derivatives (**3a** and **3b**), emissions in dichloromethane solutions appear at λ_{max} = 457 (Φ = 0.84) and 488 nm (Φ = 0.72), with Stokes shifts of 7100 and 6610 cm^{-1}, respectively. Hence, an assignment of $^3(\pi\text{-}\pi^*)$ excited states is not favored, and we tentatively assign the emission of **3a** and **3b** to originate from n → π* transitions of the (arylene-ethynylene) molecules.

Theoretical Calculations

To rationalize the differences in photoluminescent properties between *p*-$H_2N(C_6H_4C{\equiv}C)_2SiMe_3$ (**2a**) and $H(C_6H_4C{\equiv}C)_2SiMe_3$ (**2h**), the electronic structures of the ground and excited states of *p*-$H_2N(C_6H_4C{\equiv}C)_2SiH_3$ (**2a′**) and $H(C_6H_4C{\equiv}C)_2SiH_3$ (**2h′**) have been examined through

TD-DFT calculations. Previous reports have shown that rotation about the phenyl–acetylene single bond is essentially frictionless due to the cylindrical symmetry of the triple bond, which is able to maintain conjugation between the phenyl rings irrespective of the relative orientations of the aromatic planes.[27–29] This leads to the rapid equilibration and coexistence of the coplanar and twisted conformations in the ground state. Upon electronic excitation, on the other hand, changes in bond order along the C(phenyl)–C≡C fragment, from alternate single-triple bonds in the ground state (S_0) to a cumulene-type (C=C=C) bonding situation in the first singlet excited state (S_1), may afford larger energy differences between the coplanar and twisted conformations. In order to investigate how these geometric changes can affect the absorption and fluorescence spectra, three relative orientations of the phenyl rings (θ) were sampled, viz. 0°, 45°, and 90° for both the ground and the first singlet excited states of **2a′** and **2h′**, and the calculation results are reported in Tables 2 and 3, respectively.

Table 2. Computed relative energies E [eV], absorption λ_{abs} [nm], and fluorescence energies λ_F [nm] of the gas phase optimized ground and the first singlet excited state structures for **2a′** at various relative orientations of the two phenyl rings θ [°]. The oscillator strengths (f) are in the parentheses.

	S_0			S_1		
θ	0	45	90	0	45	90
E	0.000	0.027	0.047	0.00	0.047	[a]
λ_{abs}	348 (1.4521)	347 (0.8047)	350 (0.0000)			
λ_F				371 (1.6239)	378 (0.8745)	[a]

[a] Not converged.

Table 3. Computed relative energies E [eV], absorption λ_{abs} [nm], and fluorescence energies λ_F [nm] of the gas phase optimized ground and the first singlet excited state structures for **2h′** at various relative orientations of the two phenyl rings θ [°]. The oscillator strengths (f) are in the parentheses.

	S_0			S_1		
θ	0	45	90	0	45	90
E	0.000	0.021	0.043	0.00	0.010	0.063
λ_{abs}	323 (1.4804)	312 (1.1585)	281 (1.2006)			
λ_F				350 (1.5445)	337 (1.2072)	302 (1.2439)

As expected, the rotational barrier of the phenyl rings about the triple bond is very small (less than 0.047 and 0.043 eV for the ground states of **2a′** and **2h′**, respectively). At 298 K, an ensemble of rotamers should coexist in the sample. For **2h′**, as the phenyl rings rotate from a fully planar geometry to a perpendicular conformation, the extent of frontier orbital delocalization decreases (Table 4). Hence, the energy gap between the HOMO and LUMO (ΔE_{H-L}) increases from coplanar to perpendicular conformations. We note that the lowest optically active (oscillator strength $f > 0$) excitation corresponds to the HOMO → LUMO transition for all angles studied in this work. The absorption energy blue-shifts from 323 nm for the coplanar conformation to 281 nm when the two phenyl rings are perpendicular to each other. From Table 4, this transition is π → π* in nature. As the calculated absorption peaks at 323 and 312 nm with the relative phenyl ring orientations of 0° and 45° are consistent with the experimental values of 321 and 309 nm, respectively, for **2h** in *n*-hexane, we assign that these two peaks are derived from the π → π* transition.

Table 4. % Contribution of the ground state frontier molecular orbitals (FMO) of **2h′**.

θ / °	FMO (orbital energy / a.u.)	% contribution		ΔE_{H-L} / eV
0	HOMO (–0.22226)	H_3Si	2.1	4.30
		CC(1)	11.3	
		Ph(1)	33.3	
		CC(2)	26.7	
		Ph(2)	26.6	
	LUMO (–0.06374)	H_3Si	6.4	
		CC(1)	11.9	
		Ph(1)	47.0	
		CC(2)	13.8	
		Ph(2)	21.0	
45	HOMO (–0.22642)	H_3Si	2.2	4.51
		CC(1)	12.3	
		Ph(1)	34.2	
		CC(2)	27.0	
		Ph(2)	24.2	
	LUMO (–0.05997)	H_3Si	7.4	
		CC(1)	13.1	
		Ph(1)	50.2	
		CC(2)	13.2	
		Ph(2)	16.1	
90	HOMO (–0.23516)	H_3Si	3.6	4.89
		CC(1)	20.8	
		Ph(1)	46.8	
		CC(2)	23.9	
		Ph(2)	4.9	
	LUMO (–0.05468)	H_3Si	9.7	
		CC(1)	16.2	
		Ph(1)	57.8	
		CC(2)	11.4	
		Ph(2)	4.8	

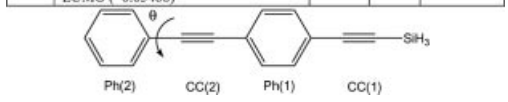

For **2a′**, the frontier orbitals are less delocalized compared with **2h′** at the angles studied (Table 5). Thus, the changes in the HOMO–LUMO energy gap are smaller for **2a′** than **2h′** along the rotation coordinate, θ. As the lowest optically active transition is derived from a HOMO → LUMO transition [except for θ = 90° where this transition is calculated to be optically inactive (f = 0)], the calculated absorption energy blue-shifts only very slightly from 348 to 347 nm at θ = 0° and 45°, respectively. Here, the character of the HOMO is dominated by the second phenylacetylene unit [CC(2) and Ph(2)] and the NH_2 group while the LUMO is mainly composed of the first phenylacetylene unit [CC(1) and Ph(1)]. This is in direct contrast to the case of **2h′**, where both the HOMO and LUMO contain major contributions from the first phenylacetylene unit [Ph(1) and CC(1)]. Since the calculated absorption wavelengths are in good agreement with the experimental value of 343 nm for **2a** in *n*-hexane, this peak is assigned to an n → π* (mixed with some π → π*) charge transfer transition.

Table 5. % Contribution of the ground state frontier molecular orbitals (FMO) of **2a′**.

θ / °	FMO (orbital energy / a.u.)	% contribution		$\Delta E_{H\text{-}L}$ / eV
0	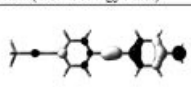 HOMO (−0.20106)	H_3Si	1.0	3.98
		CC(1)	4.8	
		Ph(1)	17.9	
		CC(2)	19.8	
		Ph(2)	38.4	
		NH_2	18.2	
	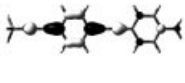 LUMO (−0.05446)	H_3Si	7.7	
		CC(1)	13.2	
		Ph(1)	49.3	
		CC(2)	12.3	
		Ph(2)	15.0	
		NH_2	2.5	
45	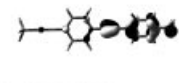 HOMO (−0.20433)	H_3Si	0.7	4.12
		CC(1)	3.4	
		Ph(1)	13.7	
		CC(2)	19.5	
		Ph(2)	42.0	
		NH_2	20.7	
	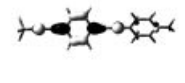 LUMO (−0.05227)	H_3Si	8.8	
		CC(1)	14.6	
		Ph(1)	52.7	
		CC(2)	11.8	
		Ph(2)	10.7	
		NH_2	1.4	
90	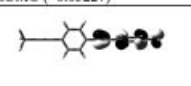 HOMO (−0.20906)	H_3Si	0.0	4.32
		CC(1)	0.0	
		Ph(1)	4.0	
		CC(2)	18.0	
		Ph(2)	50.8	
		NH_2	27.2	
	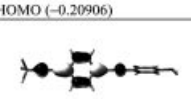 LUMO (−0.04982)	H_3Si	10.3	
		CC(1)	16.6	
		Ph(1)	57.3	
		CC(2)	11.0	
		Ph(2)	4.8	
		NH_2	0.0	

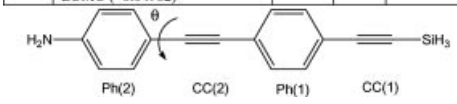

Upon excitation of **2a′** (and **2h′**) to the first singlet excited state, the molecule relaxes to a cumulene-like structure with respect to the C(phenyl)–C≡C unit, making the torsional barrier between the coplanar and perpendicular conformations higher. For instance, the rotational barrier is calculated to be 0.063 eV for the first singlet excited state (compared with 0.043 eV for the ground state) of **2h′**. The character of the HOMO and LUMO in the first singlet (S_1) excited state for **2h′** and **2a′** (Tables 6 and 7, respectively) are essentially the same as in the ground state. As the calculated emission energies of 350 and 337 nm are in good agreement with the experimental values of 347 and 324 nm measured for **2h** in *n*-hexane, these two peaks are assigned to originate from the π → π* transition. On the other hand, the calculated emission energies at 371 and 378 nm are in excellent agreement with the experimental emission of **2a** at 372 nm in *n*-hexane, and hence we assign this peak to an n → π* (mixed with some π → π*) charge transfer excited state. The proposed charge transfer nature of the fluorescence band for **2a** may explain the prominent observed solvatochromism (see above). On the contrary, **2h** displays only small spectral shifts upon changes in solvent polarity because the transition is localized in nature.

Table 6. % Contribution of the first singlet excited state frontier molecular orbitals (FMO) of **2h′**.

θ / °	FMO (orbital energy / a.u.)	% contribution		$\Delta E_{H\text{-}L}$ / eV
0	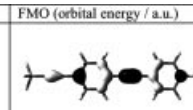 HOMO (−0.21432)	H_3Si	2.0	3.89
		CC(1)	10.9	
		Ph(1)	35.0	
		CC(2)	25.8	
		Ph(2)	26.2	
	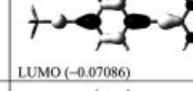 LUMO (−0.07086)	H_3Si	5.3	
		CC(1)	10.5	
		Ph(1)	45.9	
		CC(2)	14.9	
		Ph(2)	23.4	
45	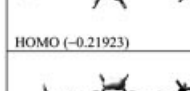 HOMO (−0.21923)	H_3Si	2.4	4.13
		CC(1)	12.9	
		Ph(1)	37.4	
		CC(2)	25.8	
		Ph(2)	21.6	
	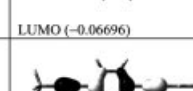 LUMO (−0.06696)	H_3Si	6.5	
		CC(1)	12.3	
		Ph(1)	50.5	
		CC(2)	14.2	
		Ph(2)	16.5	
90	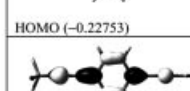 HOMO (−0.22753)	H_3Si	4.1	4.45
		CC(1)	22.8	
		Ph(1)	48.5	
		CC(2)	20.5	
		Ph(2)	4.2	
	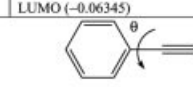 LUMO (−0.06345)	H_3Si	9.5	
		CC(1)	16.9	
		Ph(1)	58.0	
		CC(2)	11.1	
		Ph(2)	4.5	

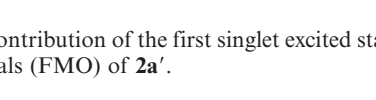

Table 7. % Contribution of the first singlet excited state frontier molecular orbitals (FMO) of **2a′**.

θ / °	FMO (orbital energy / a.u.)	% contribution		$\Delta E_{H\text{-}L}$ / eV
0	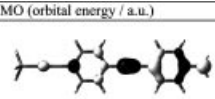 HOMO (−0.19445)	H_3Si	1.2	3.66
		CC(1)	6.0	
		Ph(1)	22.7	
		CC(2)	20.6	
		Ph(2)	34.7	
		NH_2	15.9	
	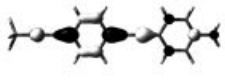 LUMO (−0.05959)	H_3Si	6.2	
		CC(1)	11.2	
		Ph(1)	47.1	
		CC(2)	13.6	
		Ph(2)	18.6	
		NH_2	3.3	
45	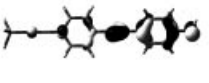 HOMO (−0.19716)	H_3Si	0.9	3.79
		CC(1)	4.4	
		Ph(1)	18.2	
		CC(2)	21.0	
		Ph(2)	38.2	
		NH_2	17.3	
	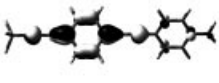 LUMO (−0.05735)	H_3Si	7.2	
		CC(1)	12.7	
		Ph(1)	51.2	
		CC(2)	13.6	
		Ph(2)	13.4	
		NH_2	1.9	

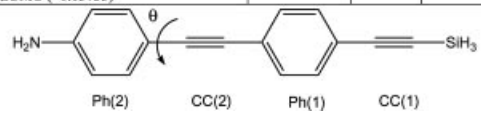

Application of Oligo(arylene-ethynylene)s for Bioconjugation

The *N*-hydroxysuccinimidyl (NHS) ester is a commonly used functional group for covalent attachment of chromo-

phoric labels to primary amino moieties (usually lysine residues) of biomolecules such as albumins, enzymes, and immunoglobulins.[30] In this work, a series of fluorescent oligo(arylene-ethynylene)s were functionalized with amine-reactive succinimidyl 4-iodobenzoate, *p*-X($C_6H_4C{\equiv}C)_n$-C_6H_4NHS [*n* = 1, X = NH_2 (**5a**), NMe_2 (**5b**), SMe (**5c**), OMe (**5d**), OH (**5e**), F (**5f**); *n* = 2, X = NH_2, NMe_2] and *p*-$Me_2NC_6H_4C{\equiv}C(C_4H_2S)C{\equiv}CC_6H_4NHS$. We have performed cytotoxicity studies of **5b** and *p*-$Me_2N(C_6H_4$-$C{\equiv}C)_2C_6H_4NHS$ on lung cancer cells, revealing that their inhibitory concentrations (IC_{50}) are higher than 100 μM, suggesting the benign nature of this class of fluorescent OPE labels toward cells. The optimal fluorophore/HSA (F/P) ratio for labeling has been determined by comparing the emission intensity of the conjugates with the intensity of a 66.6 kDa stained band in gel electrophoresis using F/P ratios of 1:1, 2.5:1, 5:1, 7.5:1 and 10:1. The emission spectra of the **5b**–**HSA** conjugate labeled with F/P ratios of 7.5:1 and 10:1 reveal the 480 nm emission band at the highest intensity. Gel electrophoresis of conjugates with different F/P ratios was performed, and the bands were stained with Coomassie Blue. Based on the brightness of the 66.6 kDa bands, the conjugation saturated at the F/P ratio of 10:1. Hence, we subsequently employed the F/P labeling ratio of 10:1 to enable complete conjugation for characterization and photophysical studies. Further increases of the F/P ratio to 20:1, 50:1 and 100:1 were performed in the protein conjugation; however, precipitation of fluorescent dyes was observed.

Characterization of (**5a**–**5f**)–**HSA** and *p*-Me_2NC_6-$H_4C{\equiv}C(C_4H_2S)C{\equiv}CC_6H_4NHS$–HSA conjugates and their degree of labeling have been investigated by MALDI-TOF mass spectrometry[31] and UV/Vis absorption spectroscopy.[32,33] The difference in molecular mass between the (**5a**–**5f**)–**HSA** conjugates and HSA (66.6 kDa) was calculated and divided by the mass of the *p*-$XC_6H_4C{\equiv}CC_6H_4$-(O)C labeling fragment to afford the mean number of fluorophores per HSA molecule (see Experimental Section). Figure 8 depicts the MALDI-TOF mass spectra of **5a**–**HSA** and **HSA**. The calculated number of **5a** and **5c**–**5f** fluorescent fragments per HSA ranges from 7.5 to 10.6, whereas that of **5b** (5.2) is lower (Figure S13).

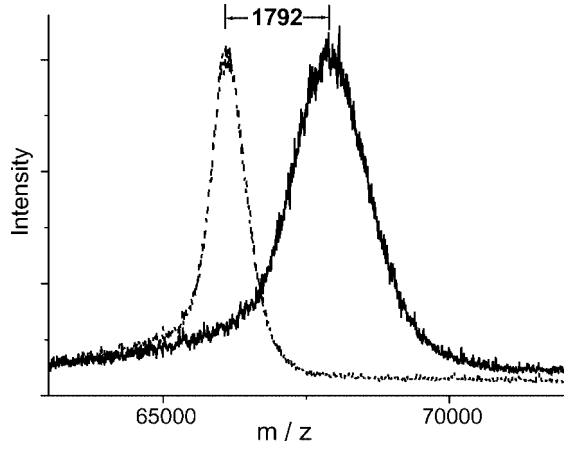

Figure 8. MALDI-TOF mass spectra of **5a**–**HSA** conjugate (——) and HSA (-----) (Δ*m*/*z* gives a labeling ratio of 7.6:1).

The degree of labeling for (**5a**–**5f**)–**HSA** can also be determined by absorption spectroscopy[32,33] with the assumption of additive absorption characteristics (see Supporting Information). The values for (**5a**–**5c**)–**HSA** are 6.4, 4.4 and 8.1, respectively, which approach the calculated ones from mass spectrometric analysis (7.6, 5.2, and 8.1, respectively). However, for (**5d**–**5f**)–**HSA**, the value obtained by the UV/Vis spectroscopic method (4.3, 5.3, and 2.7, respectively) shows a larger discrepancy from that using mass spectrometry (9.3, 7.5, and 10.6, respectively). The degree of labeling for *p*-$Me_2NC_6H_4C{\equiv}C(C_4H_2S)C{\equiv}CC_6H_4NHS$–HSA was determined by MALDI-TOF and absorption spectrometry to be 6.8 and 7.4, respectively.

Photoluminescence of Oligo(arylene-ethynylene)–HSA Conjugates

The photophysical properties of **5a**–**5f** and their HSA conjugates have been investigated (Table 1 and Supporting Information). The absorption spectra of **5a** and **5b** in CH_2Cl_2, MeCN, THF and ethyl acetate consist of two distinct peaks at 269–280 [ε = (1.24–2.42) × 10^4 $dm^3 mol^{-1} cm^{-1}$] and 354–385 nm [ε = (1.94–3.46) × 10^4 $dm^3 mol^{-1} cm^{-1}$], whereas the emission spectra show broad peaks at λ_{max} = 490–504 (**5a**) and 522–566 nm (**5b**), respectively. Both the absorption and emission bands of **5a** and **5b** are blue-shifted in protic solvents (4% DMF/H_2O and 4% DMF/PBS). The emission quantum yields of both compounds in CH_2Cl_2, THF, and ethyl acetate are in the range of 0.034–0.096, whereas those in MeCN, 4% DMF/H_2O and 4% DMF/PBS are greatly diminished (< 0.004). Upon conjugation with HSA, the emission quantum yields of **5a**–**HSA** and **5b**–**HSA** in PBS solution show a dramatic increase to 0.061 (λ_{max} = 475 nm) and 0.13 (λ_{max} = 480 nm), respectively.

Similarly, the emissions of **5c**–**5e** in aqueous medium (4% DMF in H_2O and 4% DMF in PBS) are weak (0.0017–0.059) with diminished Φ values compared to those in non-aqueous solutions. Upon conjugation with HSA, the emission exhibits a higher-energy band with enhanced Φ value (0.02–0.29). Perturbation of the photoluminescent properties therefore confirms their protein-binding capabilities. Photoluminescent properties of the *p*-$X(C_6H_4C{\equiv}C)_2$-C_6H_4NHS–HSA (X = NH_2, NMe_2) conjugates have also been examined; their absorption spectra in 4% DMF/PBS show a 278 nm band with broad shoulders at 316–358 nm, and they show less intense emissions at λ_{max} = 455 and 478 nm, respectively, compared to **5a**–**HSA** and **5b**–**HSA**. This general method for modifying OPEs into *N*-hydroxysuccinimidyl derivatives can be applied to a broader range of fluorescent dyes; for example, the thiophene counterpart has also been prepared. The absorption and emission maxima of the *p*-$Me_2NC_6H_4C{\equiv}C(C_4H_2S)C{\equiv}CC_6H_4NHS$–HSA conjugate in PBS lie at 362 and 511 nm, respectively. These values show a red shift in energy compared to the *p*-$Me_2N(C_6H_4C{\equiv}C)_2C_6H_4NHS$–HSA congener.

Acrylamide Gel Electrophoresis

These oligo(arylene-ethynylene)–HSA conjugates exhibit green fluorescence under UV irradiation. Using native gel and sodium dodecyl sulfate polyacrylamide gel electrophoresis (SDS-PAGE), (**5a**–**5f**)–**HSA** are observed to display fluorescent bands under excitation with UV light (Supporting Information) and upon staining with Coomassie Blue (Figure 9). The brightness of the fluorescent bands for the (**5a**–**5f**)–**HSA** conjugates was found to correlate with their emission quantum yields in PBS (Table 1). For instance, the fluorescence of the SMe-substituted conjugate **3c**–**HSA** is the most intense, which agrees with the highest Φ value of 0.29 in PBS.

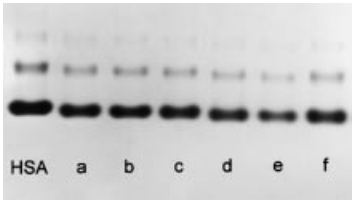

Figure 9. Native gel electrophoresis of (**5a**–**5f**)–**HSA** (marked as **a**–**f**, respectively) in 10% (w/v) polyacrylamide gel after Coomassie Blue staining.

The mobilities of the (**5a**–**5f**)–**HSA** conjugates were examined by performing the electrophoresis in parallel with HSA and a 66 kDa marker (S). The native gel and SDS-PAGE of (**5a**–**5f**)–**HSA** were stained with Coomassie Blue after electrophoresis (Supporting Information), and the (**5a**–**5f**)–**HSA** bands showed similar mobilities to unlabeled HSA. The total mass of conjugated fluorophores is insignificant in comparison to that of HSA, according to the degree of labelling described earlier, and this indicates that the mobilities of (**5a**–**5f**)–**HSA** should be close to HSA. Conjugation of **5a**–**5f** with HSA have also been verified by the coherent mobilities of (**5a**–**5f**)–**HSA** against that of the 66 kDa marker of a high-range SDS-PAGE molecular weight standard (S) (Supporting Information). The gel electrophoresis of *p*-X($C_6H_4C{\equiv}C)_2C_6H_4$NHS–HSA (X = NH_2, NMe_2) and *p*-$Me_2NC_6H_4C{\equiv}C(C_4H_2S)C{\equiv}CC_6H_4$NHS–HSA conjugates reveals similar results to those of **5a**–**HSA** and **5b**–**HSA**, although the bands are less intense.

Concluding Remarks

The photophysical properties and solvatochromic responses of a series of oligo(arylene-ethynylene)s, *p*-X($C_6H_4C{\equiv}C)_nSiMe_3$ with different chain lengths and *para* substituents have been examined. For a given *para* substituent [**1a**–**4a** (X = NH_2), **1b**–**4b** (X = NMe_2), and **1h**–**4h** (X = H)], the absorption and emission maxima show bathochromic shifts with increasing phenylene units (*n*), and linear correlations were observed for absorption or emission energies (in wavenumber) vs. 1/*n*. For compounds with NH_2 (**1a**–**4a**) and NMe_2 (**1b**–**4b**) termini, the π-π* absorptions are moderately sensitive to solvent polarity. The emission data show more discernible evidence for variations in emission maximum and quantum yield with solvent polarity; **3a** and **3b** show vibronically structured emissions in hexane at λ_{max} = 377 and 392 nm, which red-shift to 520 and 545 nm, respectively, in acetonitrile. On the contrary, very minor solvatochromic shifts are observed for **1h**–**4h**, which is consistent with the π-π* emissive excited state assignment. Using theoretical calculations, the emission of the electron-donating NH_2 derivative (**2a**) is attributed to an n → π* (mixed with some π → π*) charge transfer excited state. The nature of this distinctive transition explains the difference in solvatochromic behavior of NH_2 (**1a**–**4a**) and NMe_2 derivatives (**1b**–**4b**) compared to unsubstituted (**1h**–**4h**) counterparts. The interchange between (π-π*) and (n-π*) excited states have been achieved by varying the *para* substituent in **2c**–**2f** and **3c**–**3f**. Systematic studies on the physical (melting point increases with increasing the conjugation length) and spectroscopic properties of these OPE molecules are useful for a fundamental understanding in the area of conducting polymers.

The versatile functionalization of conjugated polymers and oligomers enables the application of biologically relevant pendants for binding DNA,[34] proteins,[35] or other biomolecules.[36] In this work, our strategy entails the esterification of oligo(arylene-ethynylene)s with the *N*-hydroxysuccinimidyl group, which reacts with lysine moieties in proteins and enables the covalent attachment of fluorophores to biomolecules. We have demonstrated that the high quantum efficiencies, large Stokes shifts (maximum 11530 cm^{-1}) and strong solvatochromism (except H- and F-substituted derivatives) of the oligo(arylene-ethynylene)s can confer rich photophysical characteristics upon the resultant bioconjugates. The absorption and emission energies could also be red-shifted by derivatizing with thiophene at the oligo(arylene-ethynylene) chain.

The (**5a**–**5f**)–**HSA**, *p*-X($C_6H_4C{\equiv}C)_2C_6H_4$NHS–HSA (X = NH_2, NMe_2) and *p*-$Me_2NC_6H_4C{\equiv}C(C_4H_2S)C{\equiv}CC_6H_4$-NHS–HSA conjugates were characterized by MALDI-TOF mass spectrometry and UV/Vis absorption spectroscopy. The optimal (**5a**–**5f**)/HSA ratio for labeling was determined to be 10:1, whereas the degree of labeling, as estimated by MALDI-TOF mass spectrometry and UV/Vis spectroscopy, were compared. The gel electrophoresis reveals green fluorescent bands for the oligo(arylene-ethynylene)–**HSA** conjugates under UV irradiation. The conjugates exhibit molecular masses that are consistent with those of HSA and a 66 kDa marker standard, thus confirming the protein-binding ability of **5a**–**5f**.

Experimental Section

General Procedures: *p*-$H_2N(C_6H_4C{\equiv}C)_2SiMe_3$[19] and *p*-$Me_2NC_6H_4C{\equiv}CH$[20] were prepared as described in the literature. $H(C_6H_4C{\equiv}C)_2SiMe_3$,[19b,21] $H(C_6H_4C{\equiv}C)_3SiMe_3$,[22] and $H(C_6H_4C{\equiv}C)_4SiMe_3$[23] were prepared by reaction of [(4-iodophenyl)ethynyl]trimethylsilane with $H(C_6H_4C{\equiv}C)_nH$ (*n* = 1, 2 and 3, respectively). Dichloromethane used for photophysical studies was washed with concentrated sulfuric acid, 10% sodium hydrogencarbonate, and water, dried with calcium chloride, and distilled from

calcium hydride. Acetonitrile used for photophysical measurements was distilled from potassium permanganate and calcium hydride. All other solvents were of analytical grade and purified according to literature methods.[37] Human serum albumin (HSA) was purchased from Sigma Chemical Co. Protein labeling experiments were performed in a 50 mM hydrogencarbonate buffer of pH = 9.0, which contained 1.59 g of Na_2CO_3 and 2.93 g of $NaHCO_3$ in 1 L of doubly distilled water. A 20 mM phosphate buffered saline (PBS) solution of pH = 7.2 was prepared by dissolving 1.25 g of Na_2HPO_4, 0.35 g of NaH_2PO_4, and 8.0 g of NaCl in 1 L of doubly distilled water. Gel permeation chromatography (GPC) was carried out using Sephadex G-25 (medium) chromatography resin from Amersham Biosciences as the stationary phase in a PD-10 desalting column (1 × 10 cm) and a 20 mM PBS solution (pH = 7.2) as eluent. High-resolution electron ionization (EI) mass spectra were obtained with a Finnigan MAT 95 mass spectrometer. ^1H (500 MHz) and ^{13}C (126 MHz) NMR spectra were recorded with a DPX 500 Bruker FT-NMR spectrometer with chemical shifts (in ppm) relative to tetramethylsilane. Elemental analyses were performed by the Institute of Chemistry at the Chinese Academy of Sciences, Beijing. Infrared spectra were recorded with a BIO RAD FTIR spectrophotometer. Thermal analyses were performed with a Perkin–Elmer TGA 7 thermogravimetric analyzer and a Perkin–Elmer DSC 7 differential scanning calorimeter (heating rate 15 °C/min, under N_2). UV/Vis spectra were recorded with a Perkin–Elmer Lambda 19 UV/Vis spectrophotometer or with a Hewlett–Packard HP8453 spectrophotometer. Matrix-assisted laser desorption ionization time-of-flight (MALDI-TOF) mass spectrometry was performed with a Finnigan Lasermat with a 337 nm nitrogen laser as the energy source.

Emission and Lifetime Measurements: Steady-state emission spectra were recorded with a SPEX 1681 Fluorolog-2 series F111AI spectrophotometer. Solution samples for measurements were degassed with at least four freeze-pump-thaw cycles. The emission spectra were corrected for monochromator and photomultiplier efficiency and for xenon lamp stability. Emission lifetime measurements were performed with an IBH FluoroCube 5000U fluorescence lifetime system (laser source with peak nominal at 295 or 373 nm and optical pulse durations <200 ps). The emission quantum yields were determined using the method of Demas and Crosby[38] with quinine sulfate in degassed 0.1 N sulfuric acid as a standard reference solution ($\Phi_r = 0.546$). Errors for λ values (±1 nm), τ (±10%), Φ (±10%) are estimated.

Computational Details: Calculations on the electronic structures of p-$H_2N(C_6H_4C{\equiv}C)_2SiMe_3$ (**2a**) and $H(C_6H_4C{\equiv}C)_2SiMe_3$ (**2h**), with the methyl groups attached to Si replaced by H atoms (herein the two model compounds are **2a′** and **2h′**), were performed using the Gaussian 03 software package.[39] A 6-31G* basis set[40,41] was used for all atoms in our calculations. Ground state geometries were fully optimized using the mPW1PW91 (one-parameter modified Perdew-Wang exchange and Perdew-Wang correlation) functional.[42] To calculate the fluorescence energies, the geometries of singlet excited-state would have to be adopted. In this regard, we used the CIS (configuration interaction with single excitations)[43] method for optimization of the geometry of the first singlet excited state. Absorption and fluorescence energies were computed at the optimized ground state and first singlet excited-state geometries, respectively, using time-dependent density functional theory (TD-DFT)[44,45] and the mPW1PW91 functional. For simplicity, no solvent has been included in our calculations; only gas phase results are given, which are expected to be compatible with the experimental results reported in non-polar solvents, such as *n*-hexane.

Labeling of Protein: Protein labeling experiments were carried out using a label/protein molar ratio of 10:1 in a 50 mM hydrogencarbonate buffer of pH = 9.0.[30a] To a solution of 0.77 mmol of NHS-capped fluorescent labels [**5a**–**5f**, p-$X(C_6H_4C{\equiv}C)_2C_6H_4NHS$ (X = NH_2, NMe_2), or p-$Me_2NC_6H_4C{\equiv}C(C_4H_2S)C{\equiv}CC_6H_4NHS$] in 50 μL of anhydrous dimethylformamide was added a stirred protein solution (5 mg of HSA in 1 mL of the hydrogencarbonate buffer). The mixture was incubated at 298 K for 5 h and was then diluted to 2.5 mL with PBS solution (20 mM, pH = 7.2). Purification of the protein conjugates was performed using gel permeation chromatography (GPC) in a 1 × 10 cm column filled with Sephadex G-25 and ca. 3.5 mL PBS (20 mM, pH = 7.2) as the eluent. A solution of ca. 3.5 mL purified label–HSA conjugate was collected.

Gel Electrophoresis: Native polyacrylamide gel electrophoresis (PAGE) analysis was performed using a 4% stacking gel and 10% resolving gel, which were prepared according to the Bio-Rad Mini-PROTEAN® 3 Cell Instruction Manual. The 10% resolving gel was prepared by mixing deionized water (6.7 mL), 40% acrylamide/bis solution (3.3 mL), and lower gel buffer [1.5 M tris(hydroxymethyl)-aminomethane, pH = 8.8, 3.3 mL]; 10% ammonium persulfate (AP, 200 μL) and *N*,*N*,*N*′,*N*′-tetramethylethylenediamine (TEMED, 10 μL) solutions were added, the mixture was stirred gently, and the solution was poured between glass plates for casting. The 4% stacking gel was prepared by mixing deionized water (3.25 mL), 40% acrylamide/bis solution (0.5 mL), upper gel buffer [0.5 M tris(hydroxymethyl)aminomethane, pH = 6.8, 1.25 mL], 10% AP (100 μL), and TEMED (10 μL). The stacking gel solution was poured between the glass plates above the resolving gel and a 10-well comb was inserted. The stacking gel was allowed to polymerize and the comb was then gently removed. The gel cassette sandwich was assembled into the inner chamber of the Mini-PROTEAN® 3 Cell system and lowered into the Mini tank. Running buffer was prepared by dissolving 3.03 g of Tris and 14.4 g of glycine in 1 L of deionized water and used to fill up the inner chamber and the Mini tank. Sample solutions were prepared by mixing solutions of labeled protein [(**5a**–**5f**)–**HSA**, p-$X(C_6H_4C{\equiv}C)_2C_6H_4NHS$–HSA (X = NH_2, NMe_2), or p-$Me_2NC_6H_4C{\equiv}C(C_4H_2S)C{\equiv}CC_6H_4NHS$–HSA] (7 μL) with Laemmli sample buffer (3 μL), and were then loaded onto the sample wells. The electrophoresis was carried out using a constant current of 70–90 mA at 200 V, and the running time was approximately 60 min. Coomassie Blue was used as a staining agent. For the denaturing sodium dodecyl sulfate polyacrylamide gel electrophoresis (SDS-PAGE), the gel preparation was similar to that of PAGE except that reducing SDS denaturant was added to the lower and upper gel buffers (0.4%, w/v), and the running buffer (0.1%).

Synthesis of p-$H_2N(C_6H_4C{\equiv}C)_nSiMe_3$ (n = 1–4; 1a–4a): 3a and **4a** were synthesized according to a procedure similar to that for p-$H_2N(C_6H_4C{\equiv}C)_2SiMe_3$ (**2a**).[19b] p-$H_2N(C_6H_4C{\equiv}C)_nH$ (1 mmol; n = 2, 3) and 1-iodo-4-(trimethylsilylethynyl)benzene (0.35 g, 1.16 mmol) were dissolved in dry THF (40 mL) under nitrogen, and Et_2NH (10 mL), $Pd(PPh_3)_2Cl_2$ (0.014 g, 0.02 mmol) and CuI (7.62×10^{-3} g, 0.04 mmol) were added. Upon stirring the reaction mixture for 24 h, the solvent was removed under reduced pressure. The product was extracted with dichloromethane (3 × 40 mL) and washed with water (2 × 30 mL). The organic phase was dried with anhydrous $MgSO_4$, concentrated under reduced pressure, and the crude product was purified by chromatography on a silica gel column using hexane/CH_2Cl_2 (2:1, v/v) as eluent.

General Procedures for Desilylation: The trimethylsilyl derivatives (**1a**–**3a**) were dissolved in CH_3OH/THF (1:1, v/v), and an equimolar amount of potassium hydroxide was added. The reaction

mixture was stirred at room temperature for 4 h, and the solvent was evaporated under reduced pressure. The product was washed with water (2×20 mL) and extracted with dichloromethane (3×40 mL). The organic phase was washed with brine (40 mL) and dried with anhydrous $MgSO_4$. The solvent was removed under reduced pressure.

3a: Pale yellow solid. Yield 0.35 g, 90%. M.p. (DSC) 234 °C. $C_{27}H_{23}NSi$ (389.57): calcd. C 83.24, H 5.95, N 3.60; found C 82.88, H 5.93, N 3.46. EI-MS: *m/z* = 389 [M^+], 374 [M^+ – Me], 344 [M^+ – Me_3]. HRMS: *m/z* (%) = 389.1603 (100), 390.1633 (39.38). ^1H NMR ($CDCl_3$): δ = 0.26 (s, 9 H, $SiMe_3$), 3.84 (br. s, 2 H, NH_2), 6.64 (d, *J* = 8.5 Hz, 2 H, C_6H_4), 7.34 (d, *J* = 8.5 Hz, 2 H, C_6H_4), 7.46 (d, *J* = 7.6 Hz, 8 H, C_6H_4) ppm. $^{13}C\{^1H\}$ NMR ($CDCl_3$): δ = –0.09 ($SiMe_3$), 87.2, 90.6, 91.2, 92.4, 96.4, 104.6, 112.3, 114.7, 122.0, 123.0, 123.2, 124.1, 131.3, 131.4, 131.5, 131.9, 133.0, 146.9 ppm. IR (KBr disc): $\tilde{\nu}$ = 2202, 2141 (m, C≡C) cm^{-1}. TGA (N_2, 15 °C/min) showed 5% weight loss at 245 °C.

4a: Pale orange solid. Yield 0.44 g, 90%. Decomposition temperature (T_d) 275 °C. $C_{35}H_{27}NSi$ (489.69): calcd. C 85.85, H 5.56, N 2.86; found C 85.47, H 5.78, N 3.09. EI-MS: *m/z* = 489 [M^+], 474 [M^+ – Me], 393 [M^+ – C≡CSiMe_3]. HRMS: *m/z* (%) = 489.1920 (100), 490.1951 (42.31). ^1H NMR ([D_8]THF): δ = 0.24 (s, 9 H, $SiMe_3$), 4.92 (br. s, 2 H, NH_2), 6.55 (d, *J* = 8.5 Hz, 2 H, C_6H_4), 7.20 (d, *J* = 8.5 Hz, 2 H, C_6H_4), 7.43–7.53 (m, 12 H, C_6H_4) ppm. $^{13}C\{^1H\}$ NMR ([D_8]THF): δ = –0.08 ($SiMe_3$), 87.0, 91.1, 91.6, 91.7, 92.1, 94.3, 96.6, 105.5, 110.8, 114.6, 122.6, 123.9, 124.2, 124.3, 124.4, 125.9, 131.8, 131.9, 132.2, 132.3, 132.4, 132.7, 133.6, 150.4 ppm. IR (KBr disc): $\tilde{\nu}$ = 2206, 2152 (m, C≡C) cm^{-1}. TGA (N_2, 15 °C/min) showed 10% weight loss at 273 °C.

Synthesis of *p*-$Me_2N(C_6H_4C{\equiv}C)_nSiMe_3$ (*n* = 1–4, 1b–4b): The procedure for *p*-$H_2N(C_6H_4C{\equiv}C)_nSiMe_3$ (**1a**–**4a**) was adopted except for using *p*-$Me_2N(C_6H_4C{\equiv}C)_nH$ (1 mmol, *n* = 1–3 for **2b**–**4b**) in the reaction with 1-iodo-4-(trimethylsilylethynyl)benzene (0.35 g, 1.16 mmol), which was followed by desilylation.

2b: Yellow solid. Yield 0.31 g, 98%. M.p. (DSC) 132 °C. $C_{21}H_{23}NSi$ (317.51): calcd. C 79.44, H 7.30, N 4.41; found C 79.09, H 7.48, N 4.53. EI-MS: *m/z* = 317 [M^+], 302 [M^+ – Me], 286 [M^+ – Me_2 – H]. HRMS: *m/z* (%) = 317.1604 (100), 318.1615 (24.81). ^1H NMR ($CDCl_3$): δ = 0.25 (s, 9 H, $SiMe_3$), 3.00 (s, 6 H, NMe_2), 6.66 (d, *J* = 9.0 Hz, 2 H, C_6H_4), 7.38–7.41 (m, 6 H, C_6H_4) ppm. $^{13}C\{^1H\}$ NMR ($CDCl_3$): δ = –0.07 ($SiMe_3$), 40.2 (NMe_2), 87.2, 92.8, 95.7, 104.9, 109.7, 111.8, 121.9, 124.3, 131.0, 131.8, 132.8, 150.2 ppm. IR (KBr disc): $\tilde{\nu}$ = 2208, 2152 (m, C≡C) cm^{-1}. TGA (N_2, 15 °C/min) showed 5% weight loss at 241 °C.

3b: Yellowish green solid. Yield 0.39 g, 93%. M.p. (DSC) 216 °C. $C_{29}H_{27}NSi$ (417.63): calcd. C 83.40, H 6.52, N 3.35; found C 83.01, H 6.64, N 3.36. EI-MS: *m/z* = 417 [M^+], 402 [M^+ – Me], 386 [M^+ – Me_2 – H], 372 [M^+ – NMe_2 – H], 345 [M^+ – $SiMe_3$ – H]. HRMS: *m/z* (%) = 417.1912 (100), 418.1940 (37.15). ^1H NMR ($CDCl_3$): δ = 0.26 (s, 9 H, $SiMe_3$), 3.00 (s, 6 H, NMe_2), 6.66 (d, *J* = 9.0 Hz, 2 H, C_6H_4), 7.41 (d, *J* = 8.9 Hz, 2 H, C_6H_4), 7.44–7.47 (m, 8 H, C_6H_4) ppm. $^{13}C\{^1H\}$ NMR ($CDCl_3$): δ = –0.09 ($SiMe_3$), 40.2 (NMe_2), 87.3, 90.5, 91.3, 93.0, 96.3, 104.7, 109.7, 111.8, 121.8, 123.0, 123.3, 124.4, 131.2, 131.4, 131.5, 131.9, 132.8, 150.3 ppm. IR (KBr disc): $\tilde{\nu}$ = 2209, 2152 (m, C≡C) cm^{-1}. TGA (N_2, 15 °C/min) showed 5% weight loss at 299 °C.

4b: Yellowish green solid. Yield 0.50 g, 97%. T_d = 306 °C. $C_{37}H_{31}NSi$ (517.75): calcd. C 85.84, H 6.03, N 2.71; found C 85.43, H 6.05, N 2.84. EI-MS: *m/z* = 517 [M^+], 502 [M^+ – Me], 486 [M^+ – Me_2 – H], 445 [M^+ – $SiMe_3$ – H]. HRMS: *m/z* (%) = 517.2228 (100), 518.2244 (24.74), 518.2280 (18.12). ^1H NMR ($CDCl_3$): δ = 0.26 (s, 9 H, $SiMe_3$), 3.00 (s, 6 H, NMe_2), 6.67 (d, *J* = 9.0 Hz, 2 H, C_6H_4), 7.41 (d, *J* = 8.9 Hz, 2 H, C_6H_4), 7.46–7.50 (m, 12 H, C_6H_4) ppm. $^{13}C\{^1H\}$ NMR ($CDCl_3$): δ = –0.07 ($SiMe_3$), 40.2 (NMe_2), 87.2, 90.5, 90.9, 91.0, 91.4, 93.0, 96.4, 104.6, 109.7, 111.8, 121.8, 122.9, 123.1, 123.2, 123.3, 124.4, 131.2, 131.4, 131.5, 131.6, 131.9, 132.8, 150.3 ppm. IR (KBr disc): $\tilde{\nu}$ = 2206, 2151 (m, C≡C) cm^{-1}. TGA (N_2, 15 °C/min) showed 5% weight loss at 295 °C.

Synthesis of $H(C_6H_4C{\equiv}C)_nSiMe_3$ (*n* = 1–4, 1h–4h): $C_6H_5C{\equiv}CSiMe_3$ (**1h**) was obtained from Aldrich Chemical Co. and used as received. $H(C_6H_4C{\equiv}C)_nSiMe_3$ (*n* = 2–4, **2h**–**4h**) were prepared according to literature methods.[21–23] *p*-$X(C_6H_4C{\equiv}C)_2SiMe_3$ [X = SMe (**2c**), OMe (**2d**), OH (**2e**), F (**2f**)] was similarly obtained by the reaction of *p*-$X(C_6H_4C{\equiv}C)H$ (1 mmol) with 1-iodo-4-(trimethylsilylethynyl)benzene (0.35 g, 1.16 mmol).

***p*-$MeS(C_6H_4C{\equiv}C)_2SiMe_3$ (2c):** White solid. Yield 0.30 g, 94%. $C_{20}H_{20}SSi$ (320.52): calcd. C 74.95, H 6.29; found C 74.58, H 6.18. EI-MS: *m/z* = 320 [M^+], 305 [M^+ – Me], 290 [M^+ – Me_2], 275 [M^+ – Me_3]. HRMS: *m/z* (%) = 320.1052 (100), 321.1078 (25.47). ^1H NMR ($CDCl_3$): δ = 0.26 (s, 9 H, $SiMe_3$), 2.50 (s, 3 H, SMe), 7.21 (d, *J* = 8.4 Hz, 2 H, C_6H_4), 7.42–7.44 (m, 6 H, C_6H_4) ppm. $^{13}C\{^1H\}$ NMR ($CDCl_3$): δ = –0.08 ($SiMe_3$), 15.3 (SMe), 89.1, 91.2, 96.2, 104.7, 119.2, 122.8, 123.4, 125.5, 125.9, 131.3, 131.9, 139.7 ppm. IR (KBr disc): $\tilde{\nu}$ = 2224, 2158 (m, C≡C) cm^{-1}.

***p*-$MeO(C_6H_4C{\equiv}C)_2SiMe_3$ (2d):** White solid. Yield 0.27 g, 89%. $C_{20}H_{20}OSi$ (304.46): calcd. C 78.90, H 6.62; found C 78.32, H 6.25. EI-MS: *m/z* = 304 [M^+], 289 [M^+ – Me], 274 [M^+ – Me_2]. HRMS: *m/z* (%) = 304.1283 (100), 305.1304 (21.23). ^1H NMR ($CDCl_3$): δ = 0.25 (s, 9 H, $SiMe_3$), 3.83 (s, 3 H, OMe), 6.88 (d, *J* = 8.7 Hz, 2 H, C_6H_4), 7.43 (s, 4 H), 7.46 (d, *J* = 8.7 Hz, 2 H, C_6H_4) ppm. $^{13}C\{^1H\}$ NMR ($CDCl_3$): δ = –0.09 ($SiMe_3$), 55.3 (OMe), 84.8, 91.4, 96.0, 104.7, 114.0, 115.1, 122.5, 123.7, 131.2, 131.8, 133.1, 159.8 ppm. IR (KBr disc): $\tilde{\nu}$ = 2217, 2158 (m, C≡C) cm^{-1}.

***p*-$HO(C_6H_4C{\equiv}C)_2SiMe_3$ (2e):** Pale yellow solid. Yield 0.27 g, 93%. $C_{19}H_{18}OSi$ (290.44): calcd. C 78.57, H 6.25; found C 78.21, H 6.05. EI-MS: *m/z* = 290 [M^+], 275 [M^+ – Me], 245 [M^+ – Me_3]. HRMS: *m/z* (%) = 290.1110 (100), 291.1147 (15.15). ^1H NMR ($CDCl_3$): δ = 0.25 (s, 9 H, $SiMe_3$), 5.03 (s, 1 H, OH), 6.80 (d, *J* = 8.4 Hz, 2 H, C_6H_4), 7.25–7.42 (m, 6 H, C_6H_4) ppm. $^{13}C\{^1H\}$ NMR ($CDCl_3$): δ = –0.08 ($SiMe_3$), 87.8, 91.2, 96.1, 104.7, 115.4, 115.6, 122.6, 123.7, 131.2, 131.9, 133.3, 155.9 ppm. IR (KBr disc): $\tilde{\nu}$ = 3467 (m, OH), 2206, 2143 (m, C≡C) cm^{-1}.

***p*-$F(C_6H_4C{\equiv}C)_2SiMe_3$ (2f):** White solid. Yield 0.28 g, 96%. $C_{19}H_{17}FSi$ (292.43): calcd. C 78.04, H 5.86; found C 78.08, H 5.51. EI-MS: *m/z* = 292 [M^+], 277 [M^+ – Me]. HRMS: *m/z* (%) = 292.1087 (100), 293.1104 (22.98). ^1H NMR ($CDCl_3$): δ = 0.26 (s, 9 H, $SiMe_3$), 7.06 (t, *J* = 8.7 Hz, 2 H, C_6H_4), 7.49–7.54 (m, 6 H, C_6H_4) ppm. $^{13}C\{^1H\}$ NMR ($CDCl_3$): δ = –0.08 ($SiMe_3$), 88.9, 90.2, 96.3, 104.6, 115.6, 115.9, 123.0, 131.3, 131.5, 131.9, 133.5 (d, *J* = 8.2 Hz), 164.3 ppm. IR (KBr disc): $\tilde{\nu}$ = 2219, 2156 (m, C≡C) cm^{-1}.

***p*-$X(C_6H_4C{\equiv}C)SiMe_3$ [X = NH_2 (a), NMe_2 (b), SMe (c), OMe (d), OH (e), F (f)]:** These compounds were synthesized by coupling reactions of 1-iodo-4-X-benzene with (trimethylsilyl)acetylene.[19b,46] Desilylation of *p*-$X(C_6H_4C{\equiv}C)SiMe_3$ according to the procedure as described in the previous section gave *p*-$X(C_6H_4C{\equiv}C)H$.

Synthesis of *p*-$X(C_6H_4C{\equiv}C)C_6H_4(O)CO{-}N(C{=}OCH_2)_2$ (5a–5f): To a solution of succinimidyl 4-iodobenzoate (0.17 g, 0.50 mmol) and *p*-$X(C_6H_4C{\equiv}C)H$ (0.50 mmol) in THF (50 mL) under nitrogen in the presence of Et_3N (20 mL) were added $Pd(PPh_3)_2Cl_2$ (14.0 mg, 0.02 mmol) and CuI (7.62 mg, 0.04 mmol). The reaction mixture was stirred at room temperature under nitrogen for 24 h. The solvent was evaporated, and the residue was purified by col-

umn chromatography (hexane/ethyl acetate, 4:1) to afford a greenish-yellow solid, **5a**–**5f**.

5a: Greenish-yellow solid. Yield: 0.16 g, 96%. $C_{19}H_{14}N_2O_4$ (334.33): calcd. C 68.26, H 4.22, N 8.38; found C 67.90, H 4.20, N 8.03. EI-MS: *m*/*z* = 334 [M^+], 220 [M^+ – ON(C=OCH_2)$_2$], 192 [M^+ – (O=C)ON(C=OCH_2)$_2$]. ^{1}H NMR ($CDCl_3$): δ = 2.92 (s, 4 H, CH_2), 3.90 (br. s, 2 H, NH_2), 6.66 (d, *J* = 8.5 Hz, 2 H, C_6H_4), 7.37 (d, *J* = 8.5 Hz, 2 H, C_6H_4), 7.60 (d, *J* = 8.5 Hz, 2 H, C_6H_4), 8.09 (d, *J* = 8.4 Hz, 2 H, C_6H_4) ppm. ^{13}C{^{1}H} NMR ([D$_8$]THF): δ = 26.3 (CH_2), 86.8, 97.0 (C≡C), 110.0, 114.6, 124.8, 131.0, 132.0, 132.2, 133.9, 150.9, 162.3, 169.9 ppm. **5a–HSA:** MS (MALDI-TOF): *m*/*z* = 67895 [MS (MALDI-TOF for HSA): *m*/*z* = 66103]. Mean number of *p*-$H_2N(C_6H_4C{\equiv}C)C_6H_4(O)C$ per HSA molecule = 7.6.

5b: Greenish yellow solid. Yield: 0.17 g, 94%. $C_{21}H_{18}N_2O_4$ (362.38): calcd. C 69.60, H 5.01, N 7.73; found C 69.22, H 5.00, N 8.13. EI-MS: *m*/*z* = 362 [M^+], 248 [M^+ – ON(C=OCH_2)$_2$], 220 [M^+ – (O=C)ON(C=OCH_2)$_2$]. ^{1}H NMR ($CDCl_3$): δ = 2.91 (s, 4 H, CH_2), 3.02 (s, 6 H, NMe_2), 6.67 (d, *J* = 9.0 Hz, 2 H, C_6H_4), 7.43 (d, *J* = 8.9 Hz, 2 H, C_6H_4), 7.59 (d, *J* = 8.6 Hz, 2 H, C_6H_4), 8.08 (d, *J* = 8.6 Hz, 2 H, C_6H_4) ppm. ^{13}C{^{1}H} NMR ($CDCl_3$): δ = 25.7 (CH_2), 40.1 (NMe_2), 86.9, 96.1 (C≡C); 108.8, 111.7, 123.1, 130.4, 131.3, 133.1, 150.6, 161.5, 169.2 ppm. IR (KBr disc): $\tilde{\nu}$ = 2211 (m, C≡C), 1764, 1741, 1597 (s, C=C, C=O) cm^{-1}. **5b–HSA:** MS (MALDI-TOF): *m*/*z* = 67476 [MS (MALDI-TOF for HSA): *m*/*z* = 66103]. Mean number of *p*-$Me_2N(C_6H_4C{\equiv}C)C_6H_4(O)C$ per HSA molecule = 5.2.

5c: Yellow solid. Yield: 0.16 g, 88%. $C_{20}H_{15}NO_4S$ (365.40): calcd. C 65.74, H 4.14, N 3.83; found C 65.52, H 4.12, N 3.62. EI-MS: *m*/*z* = 365 [M^+], 323 [M^+ – CH_2 – CO], 295 [M^+ – CH_2 – 2 CO], 251 [M^+ – ON(C=OCH_2)$_2$], 223 [M^+ – (O=C)ON(C=OCH_2)$_2$]. ^{1}H NMR ($CDCl_3$): δ = 2.51 (s, 3 H, SMe), 2.92 (s, 4 H, CH_2), 7.23 (d, *J* = 8.5 Hz, 2 H, C_6H_4), 7.47 (d, *J* = 8.5 Hz, 2 H, C_6H_4), 7.63 (d, *J* = 8.6 Hz, 2 H, C_6H_4), 8.11 (d, *J* = 8.6 Hz, 2 H, C_6H_4) ppm. ^{13}C{^{1}H} NMR ($CDCl_3$): δ = 15.2 (SMe), 25.7 (CH_2), 88.4, 93.9 (C≡C); 118.5, 124.1, 125.8, 130.3, 130.5, 131.8, 132.1, 140.6, 161.4, 169.2 ppm. **5c–HSA:** MS (MALDI-TOF): *m*/*z* = 68262 [MS (MALDI-TOF for HSA): *m*/*z* = 66103]. Mean number of *p*-$MeS(C_6H_4C{\equiv}C)C_6H_4(O)C$ per HSA molecule = 8.1.

5d: Yellow solid. Yield: 0.16 g, 92%. $C_{20}H_{15}NO_5$ (349.34): calcd. C 68.76, H 4.33, N 4.01; found C 68.76, H 4.39, N 4.33. EI-MS: *m*/*z* = 349 [M^+], 235 [M^+ – ON(C=OCH_2)$_2$], 207 [M^+ – (O=C)-ON(C=OCH_2)$_2$]. ^{1}H NMR ($CDCl_3$): δ = 2.92 (s, 4 H, CH_2), 3.85 (s, 3 H, OMe), 6.91 (d, *J* = 8.9 Hz, 2 H, C_6H_4), 7.50 (d, *J* = 8.9 Hz, 2 H, C_6H_4), 7.62 (d, *J* = 8.6 Hz, 2 H, C_6H_4), 8.10 (d, *J* = 8.6 Hz, 2 H, C_6H_4) ppm. ^{13}C{^{1}H} NMR ($CDCl_3$): δ = 25.6 (CH_2), 55.4 (OMe), 87.3, 94.3 (C≡C); 114.2, 114.4, 123.8, 130.5, 130.7, 131.6, 133.4, 160.3, 161.5, 169.2 ppm. **5d–HSA:** MS (MALDI-TOF): *m*/*z* = 68450 [MS (MALDI-TOF for HSA): *m*/*z* = 66103]. Mean number of *p*-$MeO(C_6H_4C{\equiv}C)C_6H_4(O)C$ per HSA molecule = 9.3.

5e: Yellow solid. Yield: 0.12 g, 72%. $C_{19}H_{13}NO_5$ (335.32): calcd. C 68.06, H 3.91, N 4.18; found C 68.46, H 4.08, N 3.79. EI-MS: *m*/*z* = 335 [M^+], 221 [M^+ – ON(C=OCH_2)$_2$], 193 [M^+ – (O=C)-ON(C=OCH_2)$_2$]. ^{1}H NMR ([D$_6$]DMSO): δ = 2.91 (s, 4 H, CH_2), 6.84 (d, *J* = 8.3 Hz, 2 H, C_6H_4), 7.46 (d, *J* = 8.2 Hz, 2 H, C_6H_4), 7.75 (d, *J* = 8.3 Hz, 2 H, C_6H_4), 8.10 (d, *J* = 8.1 Hz, 2 H, C_6H_4), 10.09 (s, 1 H, OH) ppm. ^{13}C{^{1}H} NMR ([D$_6$]DMSO): δ = 25.5 (CH_2), 86.5, 94.9 (C≡C); 111.4, 115.8, 122.6, 130.1, 130.2, 131.8, 133.4, 158.7, 161.2, 170.2 ppm. **5e–HSA:** MS (MALDI-TOF): *m*/*z* = 67877 [MS (MALDI-TOF for HSA): *m*/*z* = 66103]. Mean number of *p*-$HO(C_6H_4C{\equiv}C)C_6H_4(O)C$ per HSA molecule = 7.5.

5f: Yellow solid. Yield: 0.15 g, 89%. $C_{19}H_{12}NO_4F$ (337.31): calcd. C 67.66, H 3.59, N 4.15; found C 67.29, H 3.99, N 4.50. EI-MS: *m*/*z* = 337 [M^+], 223 [M^+ – ON(C=OCH_2)$_2$], 195 [M^+ – (O=C)-ON(C=OCH_2)$_2$]. ^{1}H NMR ($CDCl_3$): δ = 2.92 (s, 4 H, CH_2), 7.08 (t, *J* = 8.7 Hz, 2 H, C_6H_4), 7.53–7.57 (m, 2 H, C_6H_4), 7.64 (d, *J* = 8.5 Hz, 2 H, C_6H_4), 8.12 (d, *J* = 8.5 Hz, 2 H, C_6H_4) ppm. ^{13}C{^{1}H} NMR ($CDCl_3$): δ = 25.6 (CH_2), 88.0, 92.8 (C≡C); 115.7, 118.5, 124.3, 130.0, 130.5, 131.8, 133.8, 161.3, 164.6, 169.1 ppm. **5f–HSA:** MS (MALDI-TOF): *m*/*z* = 68641 [MS (MALDI-TOF for HSA): *m*/*z* = 66103]. Mean number of *p*-$F(C_6H_4C{\equiv}C)C_6H_4(O)C$ per HSA molecule = 10.6.

Supporting Information (see footnote on the first page of this article): Characterizations and photophysical data, DSC and TGA thermograms (Figures S1–S4); absorption and emission spectra, and correlation of absorption and emission characteristics with chain length (*n*) and solvent polarity (E_T) (Figures S5–S12). MALDI-TOF mass spectrometry (Figure S13), gel electrophoresis (Figures S14–S16), degree of labeling by UV/Vis spectroscopy.

Acknowledgments

We are grateful for financial support from the Research Grants Council of the Hong Kong SAR, China (HKU 7039/03P), The University of Hong Kong (URC-administered Seed Funding Grant 200411159082), and Area of Excellence Scheme (AoE/P-10/01) of the University Grants Committee of the Hong Kong SAR, China.

[1] a) L. A. Bumm, J. J. Arnold, M. T. Cygan, T. D. Dunbar, T. P. Burgin, L. Jones, II, D. L. Allara, J. M. Tour, P. S. Weiss, *Science* **1996**, *271*, 1705–1707; b) J. M. Tour, *Chem. Rev.* **1996**, *96*, 537–553; c) J. M. Tour, M. Kozaki, J. M. Seminario, *J. Am. Chem. Soc.* **1998**, *120*, 8486–8493; d) J. Chen, M. A. Reed, A. M. Rawlett, J. M. Tour, *Science* **1999**, *286*, 1550–1552; e) J. M. Tour, *Acc. Chem. Res.* **2000**, *33*, 791–804; f) U. H. F. Bunz, *Chem. Rev.* **2000**, *100*, 1605–1644; g) U. H. F. Bunz, *Acc. Chem. Res.* **2001**, *34*, 998–1010.

[2] a) T. Yamamoto, W. Yamada, M. Takagi, K. Kizu, T. Maruyama, N. Ooba, S. Tomaru, T. Kurihara, T. Kaino, K. Kubota, *Macromolecules* **1994**, *27*, 6620–6626; b) P. Wautelet, M. Moroni, L. Oswald, J. L. Moigne, A. Pham, J.-Y. Bigot, S. Luzzati, *Macromolecules* **1996**, *29*, 446–455; c) N. Matsumi, K. Naka, Y. Chujo, *J. Am. Chem. Soc.* **1998**, *120*, 5112–5113; d) C.-H. Lee, T. Yamamoto, *Tetrahedron Lett.* **2001**, *42*, 3993–3996.

[3] H. S. Joshi, R. Jamshidi, Y. Tor, *Angew. Chem. Int. Ed.* **1999**, *38*, 2721–2725.

[4] a) M. Leclerc, *Adv. Mater.* **1999**, *11*, 1491–1498; b) K. Maeda, N. Kamiya, E. Yashima, *Chem. Eur. J.* **2004**, *10*, 4000–4010; c) I.-B. Kim, B. Erdogan, J. N. Wilson, U. H. F. Bunz, *Chem. Eur. J.* **2004**, *10*, 6247–6254.

[5] a) E. Birckner, U.-W. Grummt, A. H. Göller, T. Pautzsch, D. A. M. Egbe, M. Al-Higari, E. Klemm, *J. Phys. Chem. A* **2001**, *105*, 10307–10315; b) C.-Z. Zhou, T. Liu, J.-M. Xu, Z.-K. Chen, *Macromolecules* **2003**, *36*, 1457–1464; c) Q. Chu, Y. Pang, *Spectrochim. Acta Part A* **2004**, *60*, 1459–1467; d) U.-W. Grummt, T. Pautzsch, E. Birckner, H. Sauerbrey, A. Utterodt, U. Neugebauer, E. Klemm, *J. Phys. Org. Chem.* **2004**, *17*, 199–206; e) K.-T. Wong, F.-C. Fang, Y.-M. Cheng, P.-T. Chou, G.-H. Lee, Y. Wang, *J. Org. Chem.* **2004**, *69*, 8038–8044.

[6] a) A. P. Davey, S. Elliott, O. O'Connor, W. Blau, *J. Chem. Soc., Chem. Commun.* **1995**, 1433–1434; b) H. Li, D. R. Powell, R. K. Hayashi, R. West, *Macromolecules* **1998**, *31*, 52–58; c) M. I. Sluch, A. Godt, U. H. F. Bunz, M. A. Berg, *J. Am. Chem. Soc.* **2001**, *123*, 6447–6448.

[7] a) T. Mangel, A. Eberhardt, U. Scherf, U. H. F. Bunz, K. Müllen, *Macromol. Rapid Commun.* **1995**, *16*, 571–580; b) C. Weder, M. S. Wrighton, *Macromolecules* **1996**, *29*, 5157–5165.

[8] a) L. S. Swanson, J. Shinar, Y. W. Ding, T. J. Barton, *Synth. Met.* **1993**, *55*, 1–6; b) S. Anderson, *Chem. Eur. J.* **2001**, *7*, 4706–4714.
[9] a) C. Weder, C. Sarwa, C. Bastiaansen, P. Smith, *Adv. Mater.* **1997**, *9*, 1035–1039; b) C. Weder, C. Sarwa, A. Montali, C. Bastiaansen, P. Smith, *Science* **1998**, *279*, 835–837.
[10] a) Q. Zhou, T. M. Swager, *J. Am. Chem. Soc.* **1995**, *117*, 12593–12602; b) D. T. McQuade, A. E. Pullen, T. M. Swager, *Chem. Rev.* **2000**, *100*, 2537–2574.
[11] a) J.-S. Yang, T. M. Swager, *J. Am. Chem. Soc.* **1998**, *120*, 5321–5322; b) J.-S. Yang, T. M. Swager, *J. Am. Chem. Soc.* **1998**, *120*, 11864–11873.
[12] T.-H. Kim, T. M. Swager, *Angew. Chem. Int. Ed.* **2003**, *42*, 4803–4806.
[13] a) S. A. Kushon, K. D. Ley, K. Bradford, R. M. Jones, D. McBranch, D. Whitten, *Langmuir* **2002**, *18*, 7245–7249; b) S. A. Kushon, K. Bradford, V. Marin, C. Suhrada, B. A. Armitage, D. McBranch, D. Whitten, *Langmuir* **2003**, *19*, 6456–6464; c) J. H. Moon, R. Deans, E. Krueger, L. F. Hancock, *Chem. Commun.* **2003**, 104–105; d) J. N. Wilson, Y. Wang, J. J. Lavigne, U. H. F. Bunz, *Chem. Commun.* **2003**, 1626–1627; e) J. H. Wosnick, C. M. Mello, T. M. Swager, *J. Am. Chem. Soc.* **2005**, *127*, 3400–3405.
[14] a) C. G. Bangcuyo, M. E. Rampey-Vaughn, L. T. Quan, S. M. Angel, M. D. Smith, U. H. F. Bunz, *Macromolecules* **2002**, *35*, 1563–1568; b) J. N. Wilson, U. H. F. Bunz, *J. Am. Chem. Soc.* **2005**, *127*, 4124–4125.
[15] D. R. Maulding, B. G. Roberts, *J. Org. Chem.* **1969**, *34*, 1734–1736.
[16] M. Levitus, K. Schmieder, H. Ricks, K. D. Shimizu, U. H. F. Bunz, M. A. Garcia-Garibay, *J. Am. Chem. Soc.* **2001**, *123*, 4259–4265.
[17] a) H. A. Dieck, F. R. Heck, *J. Organomet. Chem.* **1975**, *93*, 259–263; b) K. Sonogashira, Y. Tohda, N. Hagihara, *Tetrahedron Lett.* **1975**, *16*, 4467–4470; c) S. Takahashi, Y. Kuroyama, K. Sonogashira, N. Hagihara, *Synthesis* **1980**, 627–630.
[18] S. Huang, J. M. Tour, *Tetrahedron Lett.* **1999**, *40*, 3347–3350.
[19] a) O. Lavastre, L. Ollivier, P. H. Dixneuf, S. Sibandhit, *Tetrahedron* **1996**, *52*, 5495–5504; b) O. Lavastre, S. Cabioch, P. H. Dixneuf, J. Vohlidal, *Tetrahedron* **1997**, *53*, 7595–7604; c) C. Hortholary, C. Coudret, *J. Org. Chem.* **2003**, *68*, 2167–2174.
[20] V. Francke, T. Mangel, K. Müllen, *Macromolecules* **1998**, *31*, 2447–2453.
[21] a) E. B. Stephens, J. M. Tour, *Macromolecules* **1993**, *26*, 2420–2427; b) S.-K. Kang, H.-C. Ryu, Y.-T. Hong, *J. Chem. Soc., Perkin Trans. 1* **2001**, 736–739; c) S. M. Dirk, J. M. Tour, *Tetrahedron* **2003**, *59*, 287–293.
[22] J.-J. Hwang, J. M. Tour, *Tetrahedron* **2002**, *58*, 10387–10405.
[23] H.-Y. Chao, W. Lu, Y. Li, M. C. W. Chan, C.-M. Che, K.-K. Cheung, N. Zhu, *J. Am. Chem. Soc.* **2002**, *124*, 14696–14706.
[24] J. S. Melinger, Y. Pan, V. D. Kleiman, Z. Peng, B. L. Davis, D. McMorrow, M. Lu, *J. Am. Chem. Soc.* **2002**, *124*, 12002–12012.
[25] L. Jones, II, J. S. Schumm, J. M. Tour, *J. Org. Chem.* **1997**, *62*, 1388–1410.
[26] K. Yoshino, K. Tada, M. Onoda, *Jpn. J. Appl. Phys., Part 2* **1994**, *33*, L1785–L1788.
[27] S. Saebo, J. Almlöf, J. E. Boggs, J. G. Stark, *Theochem* **1989**, *200*, 361–373.
[28] A. V. Abramenkov, A. Almenningen, B. N. Cyvin, S. J. Cyvin, T. Jonvik, L. S. Khaikin, C. Rømming, L. V. Vilkov, *Acta Chem. Scand.* **1988**, *A42*, 674–684.
[29] V. A. Sipachev, L. S. Khaikin, O. E. Grikina, V. S. Nikitin, M. Trætteberg, *J. Mol. Struct.* **2000**, *523*, 1–22.
[30] a) G. T. Hermanson, *Bioconjugate Techniques*, Academic Press, San Diego, California, **1996**; b) E. Terpetschnig, H. Szmacinski, J. R. Lakowicz, *Anal. Biochem.* **1996**, *240*, 54–59.
[31] N. Weibel, L. J. Charbonnière, M. Guardigli, A. Roda, R. Ziessel, *J. Am. Chem. Soc.* **2004**, *126*, 4888–4896.
[32] M. Brinkley, *Bioconjugate Chem.* **1992**, *3*, 2–13.
[33] a) J. P. R. Van Dalen, J. J. Haaijman, *J. Immunol. Methods* **1974**, *5*, 103–106; b) M. W. Wessendorf, S. J. Tallaksen-Greene, R. M. Wohlhueter, *J. Histochem. Cytochem.* **1990**, *38*, 87–94.
[34] a) K. V. Gothelf, A. Thomsen, M. Nielsen, E. Cló, R. S. Brown, *J. Am. Chem. Soc.* **2004**, *126*, 1044–1046; b) M. Nielsen, A. H. Thomsen, E. Cló, F. Kirpekar, K. V. Gothelf, *J. Org. Chem.* **2004**, *69*, 2240–2250; c) C. J. Yang, M. Pinto, K. Schanze, W. Tan, *Angew. Chem. Int. Ed.* **2005**, *44*, 2572–2576.
[35] S. J. Dwight, B. S. Gaylord, J. W. Hong, G. C. Bazan, *J. Am. Chem. Soc.* **2004**, *126*, 16850–16859.
[36] J.-M. Fang, S. Selvi, J.-H. Liao, Z. Slanina, C.-T. Chen, P.-T. Chou, *J. Am. Chem. Soc.* **2004**, *126*, 3559–3566.
[37] D. D. Perrin, W. L. F. Armarego, D. R. Perrin, *Purification of Laboratory Chemicals*, 2nd Ed., Pergamon, Oxford, **1980**.
[38] J. N. Demas, G. A. Crosby, *J. Phys. Chem.* **1971**, *75*, 991–1024.
[39] M. J. Frisch, G. W. Trucks, H. B. Schlegel, G. E. Scuseria, M. A. Robb, J. R. Cheeseman, J. A. Montgomery, Jr., T. Vreven, K. N. Kudin, J. C. Burant, J. M. Millam, S. S. Iyengar, J. Tomasi, V. Barone, B. Mennucci, M. Cossi, G. Scalmani, N. Rega, G. A. Petersson, H. Nakatsuji, M. Hada, M. Ehara, K. Toyota, R. Fukuda, J. Hasegawa, M. Ishida, T. Nakajima, Y. Honda, O. Kitao, H. Nakai, M. Klene, X. Li, J. E. Knox, H. P. Hratchian, J. B. Cross, V. Bakken, C. Adamo, J. Jaramillo, R. Gomperts, R. E. Stratmann, O. Yazyev, A. J. Austin, R. Cammi, C. Pomelli, J. W. Ochterski, P. Y. Ayala, K. Morokuma, G. A. Voth, P. Salvador, J. J. Dannenberg, V. G. Zakrzewski, S. Dapprich, A. D. Daniels, M. C. Strain, O. Farkas, D. K. Malick, A. D. Rabuck, K. Raghavachari, J. B. Foresman, J. V. Ortiz, Q. Cui, A. G. Baboul, S. Clifford, J. Cioslowski, B. B. Stefanov, G. Liu, A. Liashenko, P. Piskorz, I. Komaromi, R. L. Martin, D. J. Fox, T. Keith, M. A. Al-Laham, C. Y. Peng, A. Nanayakkara, M. Challacombe, P. M. W. Gill, B. Johnson, W. Chen, M. W. Wong, C. Gonzalez, J. A. Pople, *Gaussian 03*, revision B.05, Gaussian, Inc., Wallingford, CT, **2004**.
[40] P. C. Hariharan, J. A. Pople, *Theor. Chim. Acta* **1973**, *28*, 213–222.
[41] W. J. Hehre, R. Ditchfield, J. A. Pople, *J. Chem. Phys.* **1972**, *56*, 2257–2261.
[42] C. Adamo, V. Barone, *J. Chem. Phys.* **1998**, *108*, 664–675.
[43] J. B. Foresman, M. Head-Gordon, J. A. Pople, M. J. Frisch, *J. Phys. Chem.* **1992**, *96*, 135–149.
[44] M. E. Casida, in: *Recent Advances in Density Functional Methods*, Part I (Ed.: D. P. Chong), World Scientific, Singapore, **1995**, chapter 5, p. 155–192.
[45] E. K. U. Gross, J. F. Dobson, M. Petersilka, *Top. Curr. Chem.* **1996**, *181*, 81–172.
[46] R. P. Hsung, C. E. D. Chidsey, L. R. Sita, *Organometallics* **1995**, *14*, 4808–4815.

Received: February 7, 2006
Published Online: May 10, 2006

